

MIT Open Access Articles

Measurement of differential cross sections for the production of a pair of isolated photons in pp collisions at $\sqrt{s} = 7$ TeV

The MIT Faculty has made this article openly available. **Please share** how this access benefits you. Your story matters.

Citation: Chatrchyan, S., V. Khachatryan, A. M. Sirunyan, A. Tumasyan, W. Adam, T. Bergauer, M. Dragicevic, et al. "Measurement of Differential Cross Sections for the Production of a Pair of Isolated Photons in Pp Collisions at $\sqrt{s} = 7$ TeV." Eur. Phys. J. C 74, no. 11 (November 2014).

As Published: <http://dx.doi.org/10.1140/epjc/s10052-014-3129-3>

Publisher: Springer-Verlag

Persistent URL: <http://hdl.handle.net/1721.1/94569>

Version: Final published version: final published article, as it appeared in a journal, conference proceedings, or other formally published context

Terms of use: Creative Commons Attribution



Measurement of differential cross sections for the production of a pair of isolated photons in pp collisions at $\sqrt{s} = 7$ TeV

CMS Collaboration*

CERN, 1211 Geneva 23, Switzerland

Received: 28 May 2014 / Accepted: 14 October 2014 / Published online: 12 November 2014

© CERN for the benefit of the CMS collaboration 2014. This article is published with open access at Springerlink.com

Abstract A measurement of differential cross sections for the production of a pair of isolated photons in proton–proton collisions at $\sqrt{s} = 7$ TeV is presented. The data sample corresponds to an integrated luminosity of 5.0 fb^{-1} collected with the CMS detector. A data-driven isolation template method is used to extract the prompt diphoton yield. The measured cross section for two isolated photons, with transverse energy above 40 and 25 GeV respectively, in the pseudorapidity range $|\eta| < 2.5$, $|\eta| \notin [1.44, 1.57]$ and with an angular separation $\Delta R > 0.45$, is 17.2 ± 0.2 (stat) ± 1.9 (syst) ± 0.4 (lumi) pb. Differential cross sections are measured as a function of the diphoton invariant mass, the diphoton transverse momentum, the azimuthal angle difference between the two photons, and the cosine of the polar angle in the Collins–Soper reference frame of the diphoton system. The results are compared to theoretical predictions at leading, next-to-leading, and next-to-next-to-leading order in quantum chromodynamics.

1 Introduction

The measurement of differential diphoton production cross sections offers an important test of both perturbative and non-perturbative quantum chromodynamics (QCD). At leading order (LO), diphotons are produced via quark–antiquark annihilation $q\bar{q} \rightarrow \gamma\gamma$. At next-to-leading order (NLO), diphoton production also includes the quark–gluon channel, while next-to-next-to-leading order (NNLO) adds the gluon–gluon channel, which includes a box diagram and represents a non-negligible fraction of the total cross section. Diphoton production is sensitive to the emission of soft gluons in the initial state and to the non-perturbative fragmentation of quarks and gluons to photons in the final state. Due to this rich phenomenology, theoretical predictions are challenging especially in restricted regions of phase space.

Diphoton production constitutes the major source of background in the diphoton decay channel of the newly discovered

Higgs boson [1–3], as well as to searches for physics beyond the standard model. New physics processes may also appear as non-resonant deviations from the predicted diphoton spectrum in events with large missing transverse energy, as in gauge-mediated SUSY breaking [4] or in models of universal extra dimensions [5]. Alternatively, some models predict narrow resonances, such as the graviton in the Randall–Sundrum model for warped extra dimensions [6,7].

The most recent diphoton measurements were published by the CDF and D0 Collaborations [8,9] at the Tevatron and by the ATLAS Collaboration [10] at the LHC. This paper presents an update of a previous CMS measurement at $\sqrt{s} = 7$ TeV [11] and is based on the full 2011 data sample of 5.0 fb^{-1} . It probes a phase space defined by a highly asymmetric selection for the transverse energy (E_T) of the two photons. The leading-order kinematic configuration where photons are produced back-to-back in the transverse plane is suppressed, enhancing the sensitivity to higher-order diagrams. The ratio of the NNLO to the LO prediction is increased by 20 % with respect to the previous CMS measurement [11].

The main experimental challenge for the measurement of the diphoton cross section is distinguishing the “prompt” photon signal produced either directly or as a result of fragmentation from the background that arises mainly from energetic neutral mesons, predominantly π^0 and η mesons, inside jets. These mesons typically decay to two collimated photons that are reconstructed as a single photon candidate, which is referred to as “non-prompt” in this paper. The main features used to discriminate a prompt photon from a non-prompt one are the shape of the shower measured by the electromagnetic calorimeter (ECAL) [12] and the isolation energy in a cone around the photon direction [11,13]. This information can be used to trigger on diphoton candidate events and, at the analysis level, to statistically evaluate the fraction of prompt diphoton candidates.

The particle flow (PF) event reconstruction [14] consists in reconstructing and identifying each particle with an optimal combination of all sub-detector information. In this pro-

* e-mail: cms-publication-committee-chair@cern.ch

cess, the identification of the particle type (photon, electron, muon, charged hadron, neutral hadron) plays an important role in the determination of the particle direction and energy.

In this analysis, the photon component of the PF isolation is used as the discriminating variable. The distributions of signal and background components are built from data and used in a maximum likelihood fit to estimate the signal fraction. An increased separation power with respect to previous results [11] is achieved by improving the identification and subtraction of the photon energy deposit in the isolation cone.

After a brief description of the CMS detector in Sect. 2, data and simulated samples are presented in Sect. 3, and the photon reconstruction in Sect. 4. The diphoton signal is estimated as described in Sect. 5. The number of signal events is then corrected for inefficiencies and unfolded as described in Sect. 6. Systematic uncertainties are assessed in Sect. 7, and the differential cross sections are presented and compared to theoretical predictions in Sect. 8.

2 The CMS detector

A detailed description of the CMS detector can be found elsewhere [15]. Its central feature is a superconducting solenoid, 13 m in length and 6 m in diameter, which provides an axial magnetic field of 3.8 T. The bore of the solenoid is instrumented with both the tracker (TRK) and the calorimeters. The steel flux-return yoke outside the solenoid is instrumented with gas-ionisation detectors used to reconstruct and identify muons. Charged-particle trajectories are measured by the silicon pixel and strip tracker, with full azimuthal (ϕ) coverage within $|\eta| < 2.5$, where the pseudorapidity η is defined as $\eta = -\ln[\tan(\theta/2)]$, with θ being the polar angle of the trajectory of the particle with respect to the counterclockwise beam direction. A lead tungstate crystal electromagnetic calorimeter (ECAL) and a brass/scintillator hadron calorimeter (HCAL) surround the tracking volume and cover the region $|\eta| < 3$. The ECAL barrel (EB) extends to $|\eta| < 1.479$ while the ECAL endcaps (EE) cover the region $1.479 < |\eta| < 3.0$. A lead/silicon-strip preshower detector (ES) is located in front of the ECAL endcap in the region $1.653 < |\eta| < 2.6$. The preshower detector includes two planes of silicon sensors measuring the x and y coordinates of the impinging particles. In the (η, ϕ) plane, and for $|\eta| < 1.48$, the HCAL cells map onto 5×5 ECAL crystal arrays to form calorimeter towers projecting radially outwards from points slightly offset from the nominal interaction point. In the endcap, the ECAL arrays matching the HCAL cells contain fewer crystals. A steel/quartz-fibre Cherenkov forward calorimeter extends the calorimetric coverage to $|\eta| < 5.0$.

3 Data sample

The data sample consists of proton–proton (pp) collision events collected at the LHC with the CMS detector in the year 2011, at a centre-of-mass energy (\sqrt{s}) of 7 TeV and corresponding to an integrated luminosity of 5.0 fb^{-1} .

Events are triggered [15] by requiring the presence of two photons with asymmetric transverse energy thresholds. The E_T thresholds at trigger level are 26 (18) and 36 (22) GeV on the leading (sub-leading) photon, depending on the running period. Each candidate is required to satisfy either loose calorimetric identification requirements, based on the shape of the electromagnetic shower, or loose isolation conditions. The trigger efficiency is evaluated using a tag-and-probe technique on $Z \rightarrow e^+e^-$ events [16], with electrons treated as photons. The trigger efficiency for photons selected in this analysis is measured to be between 98.8 and 100 % depending on the pseudorapidity and the interaction with the material in front of the ECAL. The total trigger efficiency is found to be constant over the data taking period.

Several samples of simulated events are used in the analysis to model signal and background processes. Drell–Yan+jets and $\gamma\gamma$ +jets signal events are generated with MADGRAPH 1.4.8 [17]. The $gg \rightarrow \gamma\gamma$ box signal process, γ +jet, and QCD dijet background processes are generated with PYTHIA 6.4.24 [18]. For all simulated samples the CTEQ6L1 [19] parton distribution functions (PDFs) are used. All generated events are then processed with PYTHIA (Z2 tune) [20] for hadronization, showering of partons and the underlying event; a detailed simulation of the CMS detector based on GEANT4 [21] is performed, and the simulated events are finally reconstructed using the same algorithms as used for the data.

The simulation includes the effects of in-time pileup (overlapping pp interactions within a bunch crossing) and out-of-time pileup (overlapping pp interactions from interactions happening in earlier and later bunch crossings) with a distribution matching that observed in data.

4 Photon reconstruction and selection

4.1 Photon reconstruction

Photon candidates are reconstructed from the energy deposits in the ECAL by grouping its channels into superclusters [22]. About half of the photons convert into an e^+e^- pair in the material in front of the ECAL. Conversion-track pairs are reconstructed from a combination of Gaussian-sum filter (GSF) electron tracks [23] and ECAL-seeded tracks fit to a common vertex and then matched to the photon candidate. The superclustering algorithms achieve an almost complete collection of the energy of such converted photons. In

the barrel region, superclusters are formed from five-crystal-wide strips in η , centred on the locally most energetic crystal (seed), and have a variable extension in the azimuthal direction (ϕ). In the endcaps, where the crystals are arranged according to an x - y rather than an η - ϕ geometry, matrices of 5×5 crystals (which may partially overlap) around the most energetic crystals are merged if they lie within a narrow ϕ road. The photon candidates are reconstructed within the ECAL fiducial region $|\eta| < 2.5$ but excluding the barrel-endcap transition regions $1.44 < |\eta| < 1.57$. This exclusion of the barrel-endcap transition regions ensures containment of the shower of the selected photon candidate in either the ECAL barrel or one of the ECAL endcaps. The fiducial region requirement is applied to the supercluster position (defined as the log-weighted barycentre of the supercluster's active channels) in the ECAL.

The photon energy is computed starting from the raw crystal energies measured in the ECAL. In the region covered by the preshower detector the energy recorded in that sub-detector is added. The variation of the crystal transparency during the run is continuously monitored and corrected using a factor based on the change in response to light from a laser and light-emitting-diode based monitoring system. The single-channel response of the ECAL is equalised by exploiting the ϕ symmetry of the energy flow, the mass constraint on the energy of the two photons in decays of π^0 and η mesons, and the momentum constraint on the energy of isolated electrons from W and Z decays. A correction factor compensates for the imperfect containment of the shower in the cluster crystals. The absolute energy scale and the residual long term drifts in the response are further corrected using $Z \rightarrow e^+e^-$ decays [22].

Interaction vertices are reconstructed from charged tracks and the vertex of the diphoton event is taken as the one with the largest sum of squared transverse momenta (Σp_T^2) of the associated tracks. The photon four-momentum is recalculated with respect to this vertex.

4.2 Photon selection

The photon candidates are first required to pass a sequence of filters that aim to remove beam backgrounds or identified detector issues and to satisfy more stringent criteria than the trigger requirements. The preselection is based on the shape of the electromagnetic shower in the ECAL and on the degree of isolation of the photon (i.e. the amount of energy deposited in the vicinity of the photon). The variables used are:

- Photon supercluster raw energy E_{SC}^{raw} : the sum of the calibrated crystal energies;
- Preshower energy E_{SC}^{ES} : the sum of the energy deposits reconstructed in the preshower detector (ES) and associated with the supercluster;

- R_9 : the energy sum of 3×3 crystals centred on the most energetic crystal in the supercluster divided by the raw energy of the supercluster;
- H/E : the ratio of the energy deposited in HCAL that is inside a cone of size $\Delta R = \sqrt{(\Delta\eta)^2 + (\Delta\phi)^2} = 0.15$ centred on the photon direction, to the supercluster energy;
- $\sigma_{\eta\eta}$: the shower transverse extension along η that is defined as:

$$\sigma_{\eta\eta}^2 = \frac{\sum (\eta_i - \bar{\eta})^2 w_i}{\sum w_i}, \quad (1)$$

where the sum runs over all elements of the 5×5 matrix around the most energetic crystal in the supercluster, and $\eta_i = 0.0174 \hat{\eta}_i$ in EB, $\eta_i = 0.0447 \hat{\eta}_i$ in EE with $\hat{\eta}_i$ denoting the index of the i th crystal along the η direction. The individual weights w_i are given by $w_i = \max(0, 4.7 + \ln(E_i/E_{5 \times 5}))$, where E_i is the energy of the i th crystal and $\bar{\eta} = \sum \eta_i E_i / \sum E_i$ is the weighted average pseudorapidity;

- $\text{Iso}_{ECAL}^{0.3}$ (ECAL isolation): the scalar sum of the E_T of the deposits in the electromagnetic calorimeter lying inside a cone of size $\Delta R = 0.3$, centred on the direction of the supercluster but excluding an inner cone of size 3.5 crystals and an η -slice region of 2.5 crystals;
- $\text{Iso}_{HCAL}^{0.3}$ (hadronic calorimeter isolation): the scalar sum of the E_T of the deposits in the hadron calorimeter that lie inside a hollow cone of outer radius of size $\Delta R = 0.3$ and inner radius of size $\Delta R = 0.15$ in the η - ϕ plane, centred on the direction of the supercluster;
- $\text{Iso}_{TRK}^{0.3}$ (tracker isolation): the scalar sum of the p_T of the tracks that are consistent with originating from the primary vertex in the event, and lie inside a hollow cone of outer radius of size $\Delta R = 0.3$ and inner radius of size $\Delta R = 0.04$ in the η - ϕ plane, centred around a line connecting the primary vertex with the supercluster but excluding an η -slice region ($\Delta\eta = 0.015$).

The isolation requirements are kept loose because the isolation is used as the discriminating variable in the signal extraction procedure. The selection criteria are defined to be slightly tighter than the trigger selection. The shower shape variables in the simulation are corrected to compensate for their imperfect modeling, mainly connected with (a) the simulation of effective readout noise in ECAL channels, (b) the effect of overlapping energy deposits from collisions in adjacent bunch crossings, and (c) the description of the material budget in the detector geometry. The correction factors are extracted from a sample of photons in $Z \rightarrow \mu^+ \mu^- \gamma$ events, and validated as a function of E_T and η in a sample of electrons from Z boson decays. The list of preselection criteria is presented in Table 1.

Table 1 List of requirements that a candidate has to satisfy to pass the analysis preselection

Variable	Requirement
Photon raw + preshower energy	$E_{SC}^{raw} + E_{SC}^{ES} > 20 \text{ GeV}$
H/E	if ($R_9 > 0.9$): $H/E < 0.082$ (EB), 0.075 (EE) if ($R_9 < 0.9$): $H/E < 0.075$
$\sigma_{\eta\eta}$	$0.001 < \sigma_{\eta\eta} < 0.014$ (EB), 0.034 (EE)
ECAL isolation in a $\Delta R = 0.3$ cone	$\text{Iso}_{ECAL}^{0.3} < 4 \text{ GeV}$ (only if $R_9 < 0.9$)
HCAL isolation in a $\Delta R = 0.3$ cone	$\text{Iso}_{HCAL}^{0.3} < 4 \text{ GeV}$ (only if $R_9 < 0.9$)
TRK isolation in a $\Delta R = 0.3$ cone	$\text{Iso}_{TRK}^{0.3} < 4 \text{ GeV}$ (only if $R_9 < 0.9$)

Table 2 List of additional requirements applied in the photon candidate selection

Variable	Requirement
Matched pixel measurements	False
H/E	$H/E < 0.05$
$\sigma_{\eta\eta}$	$\sigma_{\eta\eta} < 0.011$ (EB), 0.030 (EE)

The preselected photons must satisfy additional requirements to be considered as photon candidates. These consist of the absence of reconstructed electron track seeds in the pixel detector which match the candidate's direction, and a tighter selection on the hadronic leakage of the shower and the $\sigma_{\eta\eta}$ shower shape variable. The list of additional selection criteria is shown in Table 2.

In the simulation, prompt photons are defined as candidates satisfying the analysis selection requirements and geometrically matched to an isolated generator-level photon, either directly produced or originating from a fragmentation process. The generator-level isolation is defined as the p_T sum of stable particles in a cone of size $\Delta R = 0.4$, and is required to be less than 5 GeV.

5 Signal yield determination

The diphoton signal is extracted from events containing two photon candidates with transverse energy greater than 40(25) GeV for the leading (sub-leading) photon, and with a separation of $\Delta R > 0.45$. If more than two photon candidates are selected, the two with highest E_T are retained. The minimum separation requirement ensures that the energy deposit of one photon does not enter the isolation cone centered on the other one. The signal fraction is statistically separated from jets misidentified as photons by means of a

binned maximum likelihood fit that uses the photon component of the PF isolation as the discriminating variable.

The diphoton signal is then studied as a function of the diphoton invariant mass $m_{\gamma\gamma}$, the diphoton transverse momentum $p_T^{\gamma\gamma}$, the azimuthal angle difference $\Delta\phi_{\gamma\gamma}$ between the two photons, and the cosine of the polar angle θ^* in the Collins–Soper frame of the diphoton system [24]. A maximum likelihood fit is performed for each bin of the distributions in the above variables.

5.1 Particle flow isolation

The photon component of the PF isolation (Iso) is used to discriminate signal from background. The choice of the isolation variable is optimized to obtain the smallest total uncertainty of the measured cross section. This variable is computed, in a cone of size $\Delta R = 0.4$ around each selected photon candidate, as the E_T sum of photons reconstructed with the PF algorithm [14]. The PF isolation deals more effectively with cases of overlapping particles than the calorimetry-based isolation.

When calculating the isolation, the energy deposited by the selected photon candidate is subtracted by removing from the cone the area where the photon is expected to have deposited its energy (“footprint”), since photon energy leaking into the cone could bias the isolation sum. This is done on an event-by-event basis relying on simple geometrical considerations. The directions of the momenta of reconstructed photon candidates around the selected photon are extrapolated from the interaction vertex to the inner surface of the ECAL, and whenever they overlap with a crystal belonging to the supercluster these photon candidates are removed from the isolation sum. For the matching between the propagated trajectory and the crystal front width, a tolerance of 25 % of the face size is applied.

This procedure does not use any generator-level information and can therefore be applied in both data and simulated events.

The pile-up introduces a spurious correlation between the two candidate photons' isolation sums. For this reason the PF isolation sums for both photons are corrected, event by event, for the presence of pile-up with a factor proportional to the average pile-up energy density (ρ) calculated with FASTJET [25].

5.2 Template construction

The diphoton signal is extracted through a two-dimensional binned maximum likelihood fit that uses the isolation of the two selected photon candidates as discriminating variables. Different templates are built for the prompt–prompt (f_{pp}), prompt–non-prompt (f_{pn}), non-prompt–prompt (f_{np}), and non-prompt–non-prompt (f_{nn}) components in the (Iso)₁,

Iso₂) plane, where Iso₁ and Iso₂ represent the isolation variables for the two selected photon candidates in the event. The probability distribution function has the following form:

$$\begin{aligned} \mathcal{P}_{2D}(\text{Iso}_1, \text{Iso}_2) &= f_{pp}T_{pp}(\text{Iso}_1, \text{Iso}_2) + f_{pn}T_{pn}(\text{Iso}_1, \text{Iso}_2) \\ &+ f_{np}T_{np}(\text{Iso}_1, \text{Iso}_2) + f_{nn}T_{nn}(\text{Iso}_1, \text{Iso}_2) \end{aligned} \quad (2)$$

where $T_{kk}(\text{Iso}_1, \text{Iso}_2)$ is the function describing the isolation distribution (template) for the component f_{kk} . Techniques have been developed to extract the templates from data to avoid possible biases coming from an imperfect modeling of the events in the simulation. Samples of events where at least one photon passes the photon selection are used to create prompt–prompt, prompt–non-prompt, non-prompt–prompt and non-prompt–non-prompt templates with high statistical precision, as described in the following.

The “random cone” technique is used to extract the prompt photon template with high statistical accuracy. In this procedure we compute the isolation energy in a region separated from the candidate photon. Starting from the photon (η, ϕ) axis, a new axis is defined at the same pseudorapidity η but with a random separation in azimuthal angle ϕ_{RC} between 0.8 and $2\pi - 0.8$ radians from the photon ϕ . This new axis is used to define the random cone provided that no jet with $p_T > 20$ GeV or photon or electron with $p_T > 10$ GeV is reconstructed within $\Delta R < 0.8$ and no muon is reconstructed within $\Delta R < 0.4$ from this axis. In the case where the new axis does not meet these requirements, a new azimuthal angle is generated. The isolation energy, which is defined as the energy collected in a cone of size $\Delta R < 0.4$ about the new axis once the fraction corresponding to the area of the photon supercluster has been removed, is then used to populate the prompt photon template.

The distribution of the template variable has been studied in $Z \rightarrow e^+e^-$ events and found to be in agreement with the template built with the random cone technique.

The background (non-prompt) template cannot be defined by simply inverting the photon preselection, because the candidates entering the analysis, i.e. fulfilling the preselection requirements, have “photon-like” characteristics, while the set of candidates not fulfilling the photon preselection criteria includes a large number of genuine jets. To avoid this bias, the candidates selected to populate the non-prompt photon template are chosen from those that fulfil all the photon selection criteria, except the $\sigma_{\eta\eta}$ shower shape, which is not strongly correlated with the isolation variable as a result of the footprint removal technique described in the previous section. The events in a “sideband” close to the photon selection criterium are used to populate the non-prompt photon template. The sideband is defined as $0.011 < \sigma_{\eta\eta} < 0.014$ for candidates reconstructed in the ECAL barrel and $0.030 < \sigma_{\eta\eta} < 0.034$ for candidates reconstructed in the ECAL endcaps.

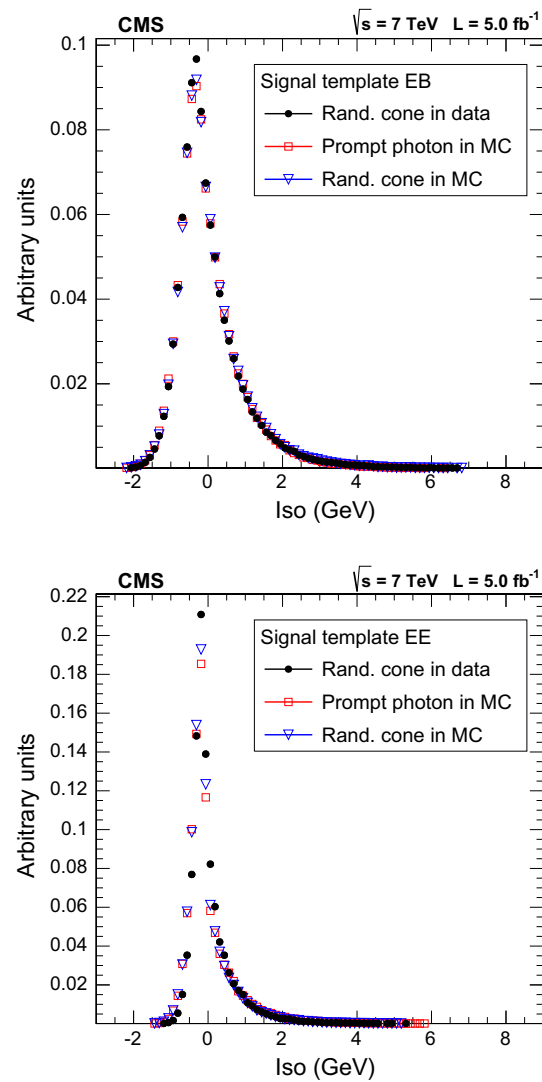


Fig. 1 Comparison of prompt photon templates in data and simulation: prompt photons in the simulation (*squares*), prompt photon templates extracted with the random cone technique from simulation (*triangles*) and from data (*dots*); (*top*) candidates in the ECAL barrel, (*bottom*) candidates in the ECAL endcaps. All histograms are normalized to unit area

The same procedure (Sect. 5.1) is used for subtracting the pile-up energy from the photon isolation sums. The templates obtained using the random cone and the sideband techniques in the simulation are compared with the one-dimensional PF isolation distribution for prompt and non-prompt photons in simulated events and with the templates obtained from data (Figs. 1, 2).

The residual differences in the simulation between the isolation distribution and the templates defined with the random cone and the sideband techniques are accounted for as systematic uncertainties on the template shapes.

The two-dimensional templates are built selecting candidate photons from data with the same kinematics as the

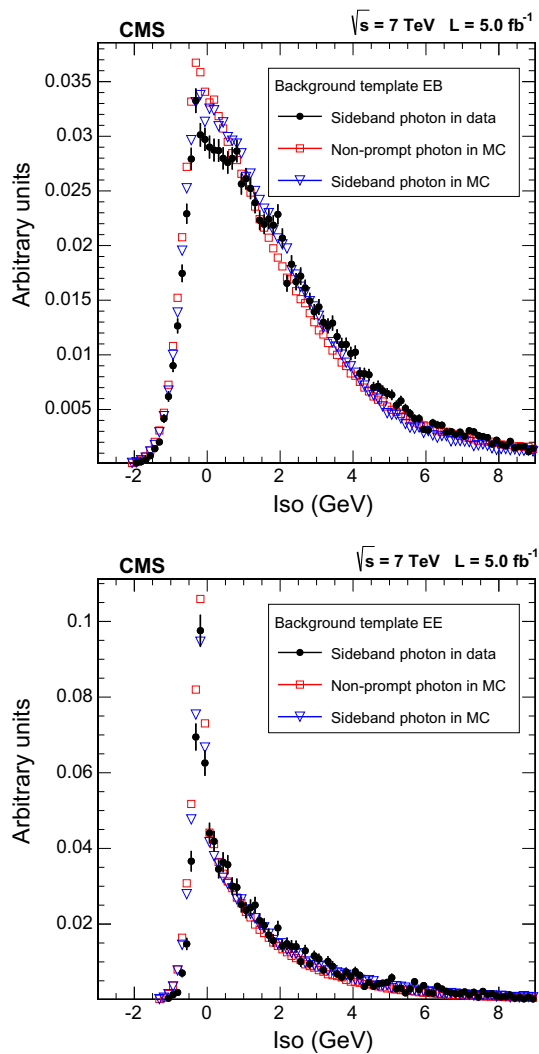


Fig. 2 Comparison of non-prompt photon templates in data and simulation: non-prompt photons in the simulation (*squares*), non-prompt photon templates extracted with the sideband technique from simulation (*triangles*) and from data (*dots*); (*top*) candidates in the ECAL barrel, (*bottom*) candidates in the ECAL endcaps. All histograms are normalized to unit area

diphoton events to be fitted. The procedure presented below correctly models the isolation distribution even in the case of overlap between the isolation cones of the two photon candidates.

The prompt–prompt template is built from events where the pileup energy density matches that of the event to be fitted, and where the two random cone directions are found having the same pseudorapidity and the same azimuthal angular separation as the selected photons.

The prompt–non-prompt template is built from events where a sideband photon is selected. The isolation sum around the sideband photon is used for the candidate to be fitted under the non-prompt-hypothesis. A direction satisfying the random cone criteria is then searched for in the same tem-

plate event (oriented as the second candidate in the selected diphoton event) and used to calculate the isolation sum for the candidate to be fitted under the prompt hypothesis.

The non-prompt–non-prompt template is built selecting two events, each of which contains one sideband photon and such that their orientation matches the orientation of the candidate photons in the event to be fitted. Then, depending on the fraction of photon candidates with $\Delta R_{\gamma\gamma} < 1.0$ present in the bin of the observable under analysis, a choice between two different strategies is made. If the fraction is below 10 %, the effect of the overlapping isolation cones can be neglected. The two-dimensional non-prompt–non-prompt template is then built by calculating each of the two isolation sums in the separate events. If the fraction is above 10 %, an additional requirement is imposed: the sum of the FastJet ρ of the two selected template events has to match the one of the diphoton event to be fitted. Then, the sets of reconstructed particles in the two template events are merged, and the isolation sums are calculated from this merged set of reconstructed particles along the direction of each sideband photon.

In this procedure, the pileup energy density of the template events is used to model the pileup energy density of the event to be fitted, and this allows us to describe the correlation between the isolation sums. The effect of the residual correlation mis-modeling is added to the template shape systematic uncertainty in the final result.

5.3 Fitting technique

The fit is performed separately for the cases where both candidates are reconstructed in the ECAL barrel, one in the ECAL barrel and one in the ECAL endcaps, or both in the ECAL endcaps. If both candidates are in the same detector region (EB-EB and EE-EE categories), the leading selected photon is assigned randomly to axis 1 or 2 of the two-dimensional plane, and the prompt–non-prompt (f_{pn}) and non-prompt–prompt (f_{np}) fractions are constrained to have the same value.

The fit, performed in each bin of the differential variables, is restricted to the region where the isolation of the photons is smaller than 9 GeV. To guarantee its stability even in the less populated bins, the fit is performed in steps. First the size of the bins in the two-dimensional plane ($\text{Iso}_1, \text{Iso}_2$) is optimised to reduce statistical fluctuations of template shape in the tails; then a first fit is performed on the projections of the isolation distributions on the two axes of the plane using the one-dimensional templates described above. In a subsequent step, the fractions of prompt–prompt, prompt–non-prompt, non-prompt–prompt, and non-prompt–non-prompt, which are constrained to sum up to unity, are fit in the two-dimensional plane using as a constraint the results of the previous fit. The final likelihood maximisation is then performed after removing all constraints, and using as ini-

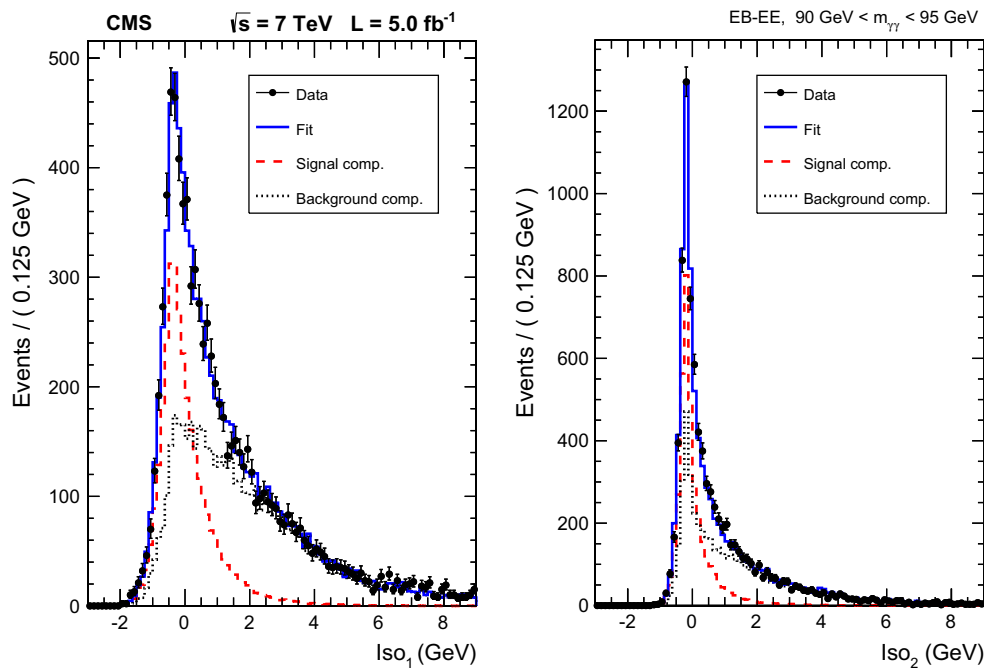


Fig. 3 Result of the first step of the fitting procedure, for the $90 \text{ GeV} < m_{\gamma\gamma} < 95 \text{ GeV}$ bin in the EB-EE category: isolation distribution for the photon reconstructed in the (left) ECAL barrel, (right) ECAL endcaps

tial values of the parameters those found in the previous step.

An example of the first step of the procedure is obtained by fitting the one-dimensional projections of the isolation distributions as shown in Fig. 3. An example of the results of the final two-dimensional fit (projected on the axes for the sake of clarity) is shown in Fig. 4. The fractions of prompt–prompt, prompt–non-prompt, and non-prompt–non-prompt components are shown in Fig. 5 for the observables of the differential analysis. We fit about 69000 prompt diphoton events in the whole acceptance of the analysis.

The reported purity suffers from a contamination of electrons coming predominantly from Drell–Yan e^+e^- and incorrectly reconstructed as photons. The contamination is most significant in the Z peak region, where it reaches about 25 % of the raw diphoton yield. The fraction of electron pairs passing the analysis selection and contributing to the prompt–prompt fitted fraction is estimated from simulation, where correction factors are applied to obtain the electron to photon mis-identification probability measured in data, and used to subtract the contamination.

6 Efficiencies and unfolding

Following the methodology presented in the previous sections, a “raw” diphoton production cross section is extracted. To obtain the final result, this cross section is corrected for inefficiencies and finally unfolded from the measured quantities to the corresponding particle-level quantities.

The total diphoton efficiency can be separated into the trigger efficiency and reconstruction/selection efficiency, and can be written as:

$$\epsilon_{\gamma\gamma} = \epsilon_{\text{trig}} \times \epsilon_{\text{sel}} \times C_{\gamma 1}^{Z \rightarrow e^+e^-} \times C_{\gamma 2}^{Z \rightarrow e^+e^-} \times C_{\gamma 1}^{Z \rightarrow \mu^+\mu^- \gamma} \times C_{\gamma 2}^{Z \rightarrow \mu^+\mu^- \gamma},$$

where ϵ_{trig} is the trigger efficiency and ϵ_{sel} is the diphoton reconstruction/selection efficiency from simulation. The factors $C_{\gamma 1}^{Z \rightarrow e^+e^-}$ and $C_{\gamma 2}^{Z \rightarrow e^+e^-}$ are the corrections to the efficiency for each photon candidate to pass all the selection requirements except the electron veto; $C_{\gamma 1}^{Z \rightarrow \mu^+\mu^- \gamma}$ and $C_{\gamma 2}^{Z \rightarrow \mu^+\mu^- \gamma}$ are the corrections to the electron veto efficiency.

The values of the correction factors are determined from the ratio of the efficiency in data to that in the simulation, measured with a tag-and-probe method using (i) samples of $Z \rightarrow e^+e^-$ for the full selection except the electron-veto requirement, and (ii) samples of photons from the final-state-radiation of $Z \rightarrow \mu^+\mu^- \gamma$ for the electron-veto requirement.

The diphoton reconstruction/selection efficiency ϵ_{sel} is about 85 % when both photons are in the barrel, 75 % when one photon is in the barrel and the other in one endcap, and 64 % when both photons are in the endcaps. All these correction factors are estimated from data and range from 0.99 to 1.02, depending on the photon E_T and η .

The detector effects are unfolded from the measured yields for a direct comparison of experimental measurements with theoretical predictions. The number of unfolded diphoton events in each bin of the differential observables is

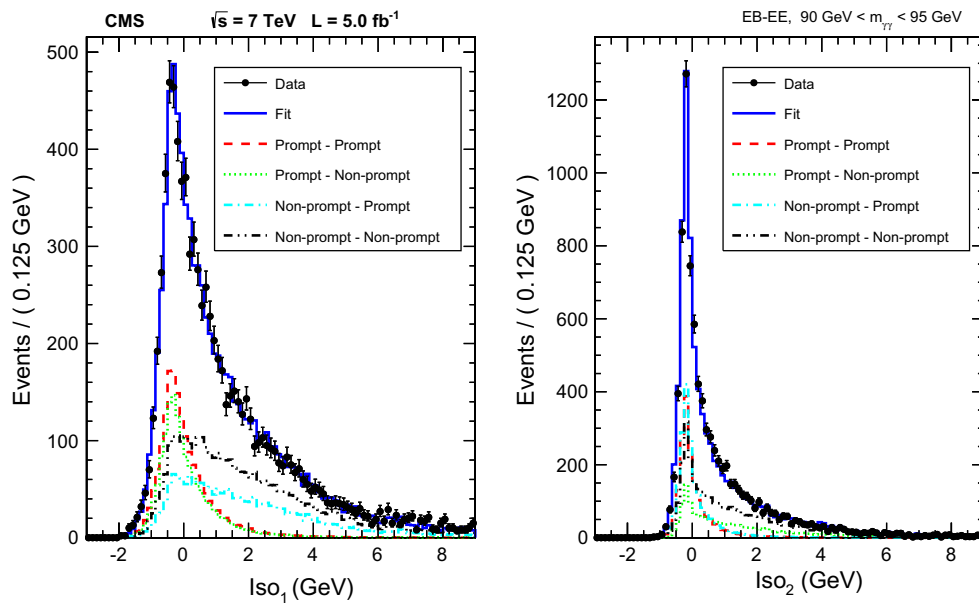


Fig. 4 Projections of the result of the final step of the fitting procedure, for the $90 \text{ GeV} < m_{\gamma\gamma} < 95 \text{ GeV}$ bin in the EB-EE category: isolation distribution for the photon reconstructed in the (left) ECAL barrel, (right) ECAL endcaps

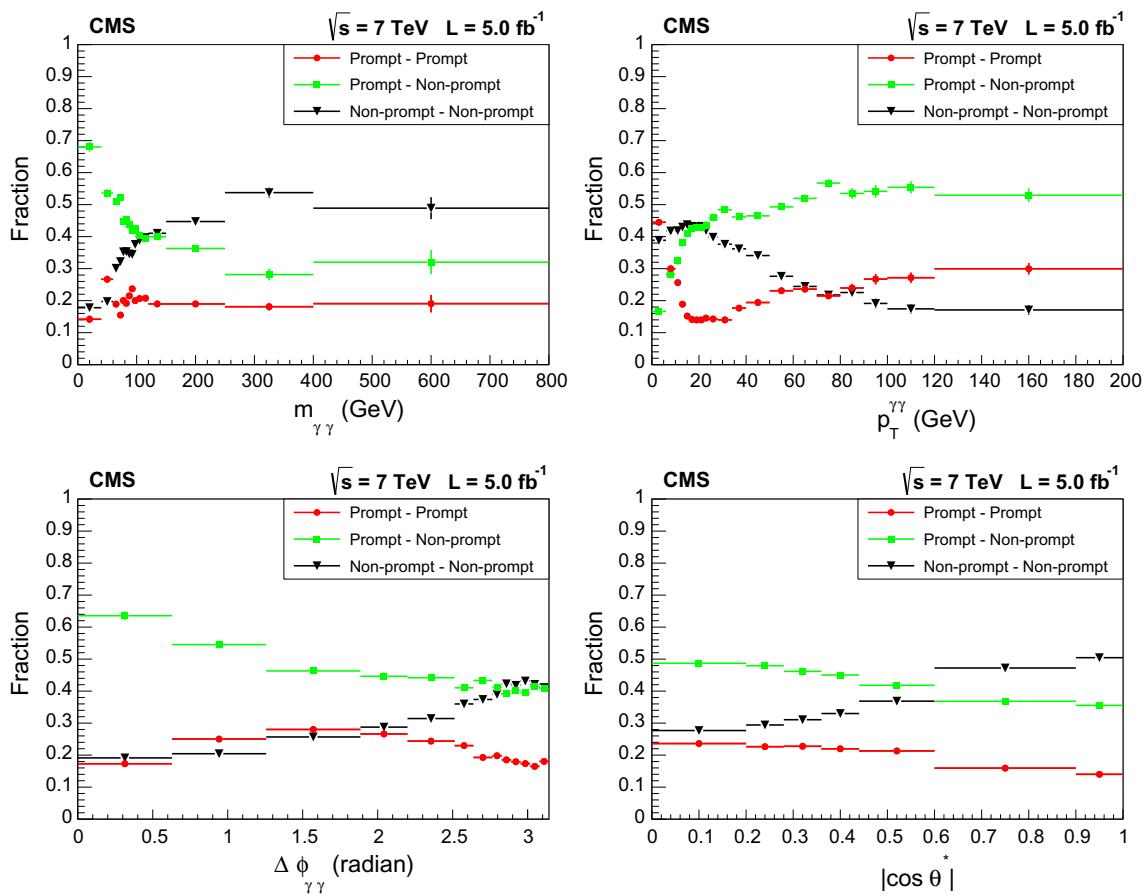


Fig. 5 Fractions of prompt–prompt, prompt–non-prompt and non-prompt–non-prompt components as a function of $m_{\gamma\gamma}$, $p_T^{\gamma\gamma}$, $\Delta\phi_{\gamma\gamma}$, $|\cos\theta^*|$ in the whole acceptance of the analysis. Uncertainties are statistical only

obtained from the reconstructed diphoton events in the data, $\mathbf{N}_{\text{GEN}}^{\text{data}} = M^{-1} \times \mathbf{N}_{\text{RECO}}^{\text{data}}$, where the unfolding matrix M is obtained from simulation, $\mathbf{N}_{\text{RECO}}^{\text{MC}} = M \times \mathbf{N}_{\text{GEN}}^{\text{MC}}$. The unfolding matrix is calculated using the iterative Bayesian technique [26, 27]. The diphoton simulated sample from MADGRAPH hadronized with PYTHIA is used. The distributions of diphoton candidates in the simulation are reweighted to the distributions of the raw diphoton yields from data as obtained from the fit procedure, for all the observables. The difference between the weighted and unweighted results is taken into account as a systematic uncertainty, and amounts to about 1 %. The unfolding correction amounts to 7 % of the raw yield at maximum, for the bins where the slope of the kinematic distributions is the steepest.

7 Systematic uncertainties

Table 3 summarises the main sources of systematic uncertainty in the measurement of the integrated cross section.

The dominant uncertainty in the template shapes arises from the difference in shape between the templates built with the techniques described in Sect. 5 and the distributions of the isolation variable for prompt or non-prompt isolated photons for simulated events. The latter are used to generate data samples for each bin of the differential variables, with the fractions measured in data. Then, each of these datasets is fitted with templates built in the simulation with the same techniques used on data, and the average difference between the fitted fractions and those used for the generation is quoted as a systematic uncertainty. It amounts to 3 % (barrel template) and 5 % (endcap template) for the prompt component, and between 5 % (barrel template) and 10 % (endcap template) for the non-prompt component. The uncertainty in the template shape for fragmentation photons is evaluated in the simulation by doubling the probability of the fragmentation process, and that yields an additional 1.5 % uncertainty in the measured cross section. In the case of the non-prompt-non-

prompt template, and only for the bins where a significant fraction of the diphoton candidates are close in $\Delta R_{\gamma\gamma}$, an additional uncertainty ranging from 3 to 5 % is introduced to account for the imperfections on the template shape description due to the effect of ECAL noise and PF thresholds on the combination of two different events to build the template.

The systematic uncertainty arising from the statistical uncertainty in the shape of the templates is evaluated generating modified templates, where the content of each bin is represented by a Gaussian distribution centred on the nominal bin value and with standard deviation equal to the statistical uncertainty of the bin. The root mean square of the distribution of the fitted purity values, divided by the purity measured with the original template, is used as systematic uncertainty in the purity measurement and amounts to about 3 %.

A possible bias associated with the fitting procedure is evaluated using pseudo-experiments. Pseudo-data samples are generated with given fractions of prompt–prompt, prompt–non-prompt, and non-prompt–non-prompt contributions, using the templates from simulation as generator probability density functions. Each data sample is then fitted with the same templates used for the generation. The average bias is negligible in all bins.

The systematic uncertainty associated with the subtraction of Drell–Yan e^+e^- events is evaluated by propagating the uncertainty in the electron to photon misidentification probability to the subtracted yield. The uncertainty in the fraction of such events that is fitted as prompt–prompt is also taken into account. This contribution is maximal for $m_{\gamma\gamma}$ close to the Z-boson mass. The relative contribution to the total systematic uncertainty is below 0.5 %.

The systematic uncertainty in the trigger efficiency is found to be below 0.5 %. The systematic uncertainty in the reconstruction and selection efficiencies is dominated by the uncertainty in the data-to-simulation corrections from the $Z \rightarrow e^+e^-$ and $Z \rightarrow \mu^+\mu^-\gamma$ control samples, and it ranges from 2 % in the barrel to 4 % in the endcap.

The systematic uncertainty in the integrated luminosity that corresponds to our data sample is 2.2 % [28].

The total systematic uncertainty in the measurement amounts to approximately 8 % when both candidates are reconstructed within the ECAL barrel, and to 11 % for the full acceptance of the analysis.

Table 3 Sources of systematic uncertainty in the measurement of integrated cross section

Source of uncertainty	
Prompt template shape (EB)	3 %
Prompt template shape (EE)	5 %
Non-prompt template shape (EB)	5 %
Non-prompt template shape (EE)	10 %
Effect of fragmentation component	1.5 %
Template statistical fluctuation	3 %
Selection efficiency	2–4 %
Unfolding procedure	1 %
Integrated luminosity	2.2 %

8 Results and comparison with theoretical predictions

The measured unfolded differential cross sections are compared with the following generators for QCD diphoton production: SHERPA 1.4.0 [29], DIPHOX 1.3.2 [30] supplemented with GAMMA2MC 1.1 [31], RESBOS [32, 33], and 2γ NNLO [34]. Predictions with SHERPA are computed at LO for the Born contribution with up to three additional real emissions

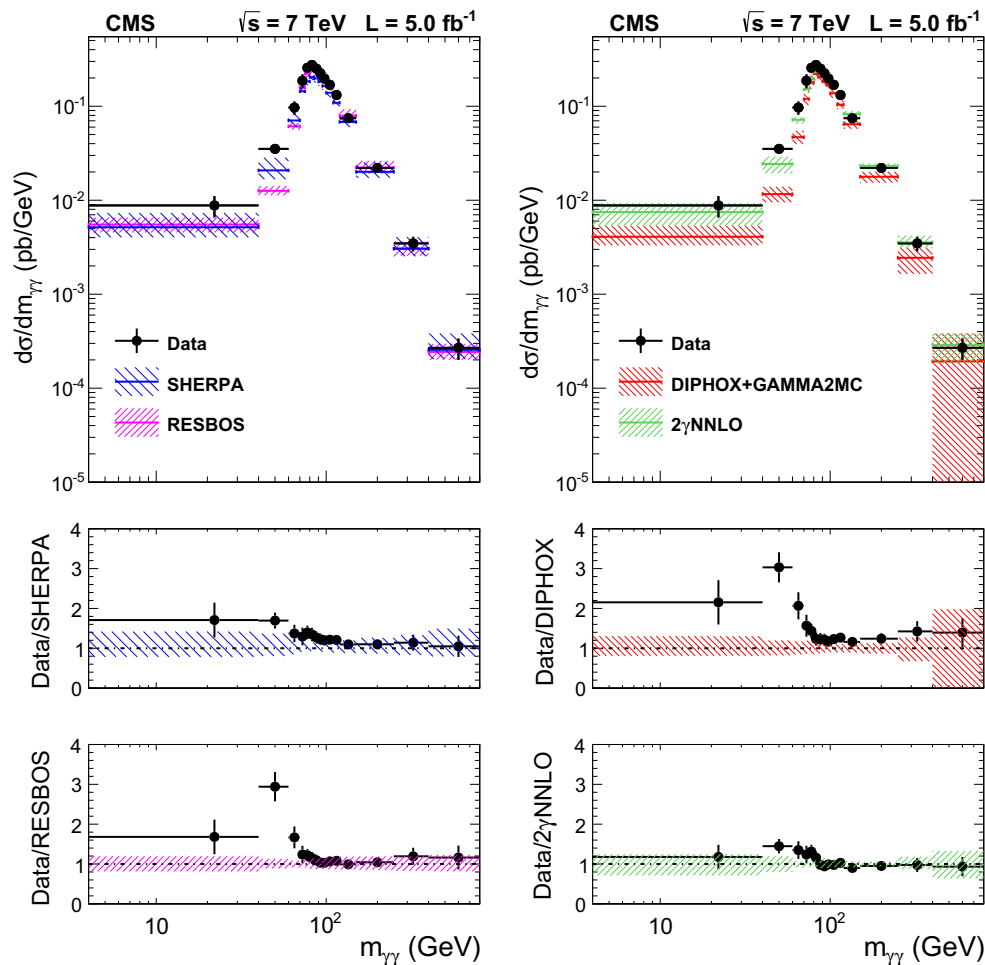


Fig. 6 The comparisons of the differential cross section between data and the SHERPA, DIPHOX + GAMMA2MC, RESBOS, and 2γ NNLO predictions for $m_{\gamma\gamma}$. *Black dots* correspond to data with *error bars* including all statistical and systematic uncertainties. Only the scale uncertainty

is included for the SHERPA prediction. Scale, PDF and α_S uncertainties are included for DIPHOX + GAMMA2MC and RESBOS. Only statistical and scale uncertainties are included for the 2γ NNLO prediction

(three extra jets) and with the box contribution at the matrix element level. The DIPHOX NLO generator includes the direct and fragmentation contributions and uses a full fragmentation function for one or two partons into a photon at NLO. The direct box contribution, which is formally part of the NNLO corrections since it is initiated by gluon fusion through a quark loop, is computed at NLO with GAMMA2MC. The RESBOS NLO generator features resummation for Born and box contributions, and effectively includes fragmentation of one quark/gluon to a single photon at LO. The latter process is regulated to avoid divergences and does not include the full fragmentation function. The RESBOS $p_T^{\gamma\gamma}$ spectrum benefits from a soft and collinear gluon resummation at next-to-next-to-leading-log accuracy. 2γ NNLO predicts the direct $\gamma\gamma+X$ processes at NNLO. The SHERPA sample is used after hadronization while DIPHOX + GAMMA2MC, RESBOS, and 2γ NNLO are parton-level generators only and cannot be interfaced with parton shower generators.

The predictions have been computed for the phase space $E_T^{\gamma 1} > 40$ GeV, $E_T^{\gamma 2} > 25$ GeV, $|\eta_\gamma| < 1.44$ or $1.57 < |\eta_\gamma| < 2.5$, $\Delta R(\gamma_1, \gamma_2) > 0.45$. An isolation requirement is applied at the generator level. In SHERPA, the E_T sum of stable particles in a cone of size $\Delta R = 0.4$ has to be less than 5 GeV (after hadronization). In DIPHOX, GAMMA2MC, and RESBOS the E_T sum of partons in a cone of size $\Delta R = 0.4$ is required to be less than 5 GeV. In 2γ NNLO, the smooth Frixione isolation [35] is applied to the photons to suppress the fragmentation component:

$$E_T^{\text{Iso}}(\Delta R) < \epsilon \left(\frac{1 - \cos(\Delta R)}{1 - \cos(\Delta R_0)} \right)^n, \tag{3}$$

where E_T^{Iso} is the E_T sum of partons in a cone of size ΔR , $\Delta R_0 = 0.4$, $\epsilon = 5$ GeV, and $n = 0.05$. This criterion, tested with DIPHOX, is found to have the same efficiency as that used for the other generators within a few percent. A non-perturbative correction is applied to DIPHOX, GAMMA2MC,

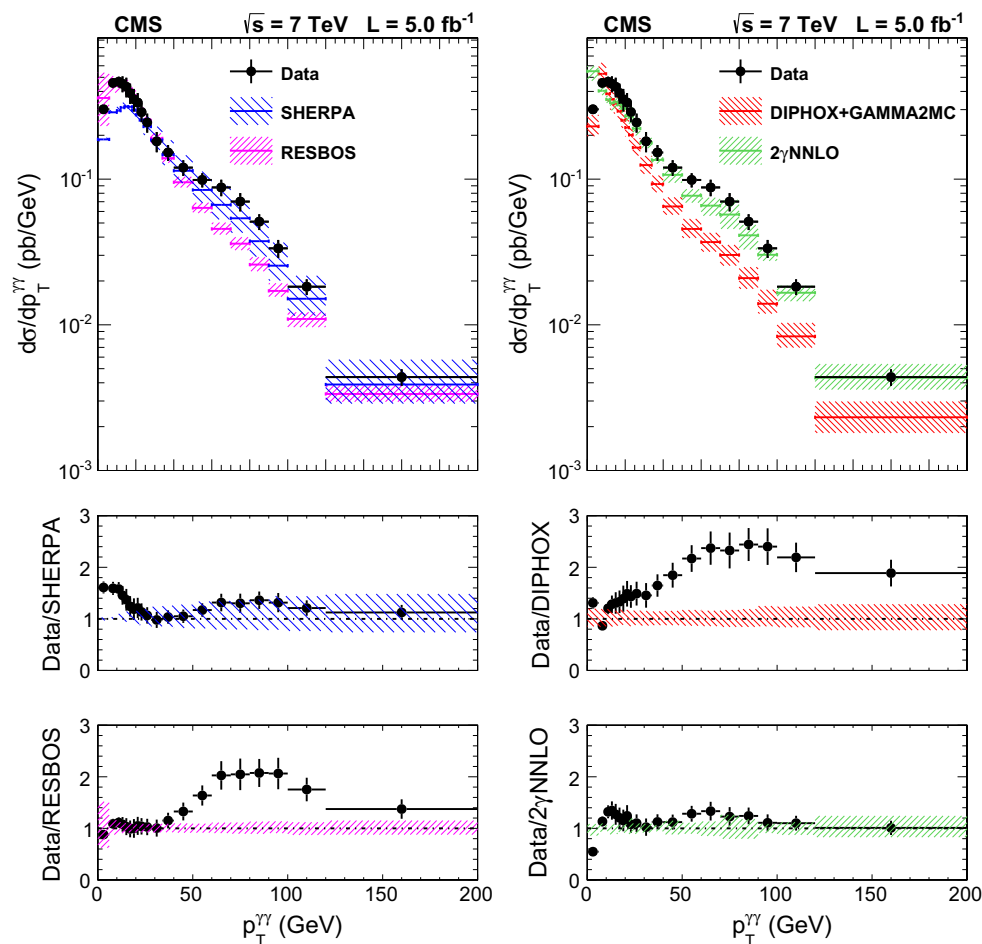


Fig. 7 The comparisons of the differential cross section between data and the SHERPA, DIPHOX + GAMMA2MC, RESBOS, and 2γ NNLO predictions for $p_T^{\gamma\gamma}$. *Black dots* correspond to data with *error bars* including all statistical and systematic uncertainties. Only the scale uncertainty

is included for the SHERPA prediction. Scale, PDF and α_S uncertainties are included for DIPHOX + GAMMA2MC and RESBOS. Only statistical and scale uncertainties are included for the 2γ NNLO prediction

and 2γ NNLO predictions to correct for the fact that those generators do not include parton shower or underlying event contributions to the isolation cone. The fraction of diphoton events not selected due to underlying hadronic activity falling inside the isolation cone is estimated using the PYTHIA 6.4.22 [18] event generator with tunes Z2, D6T, P0, and DWT [20]. A factor of 0.95 ± 0.04 is applied to the parton-level cross section to correct for this effect.

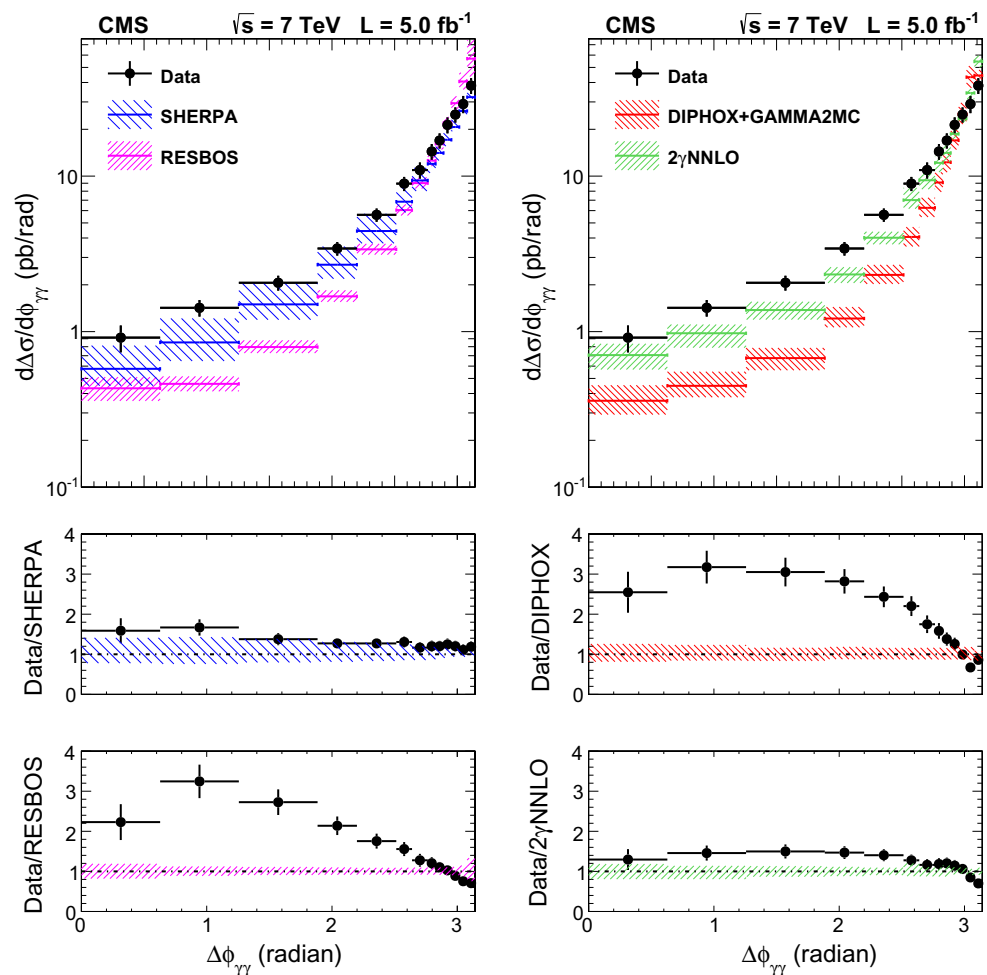
Theoretical predictions are performed using the CT10 [36] NLO PDF set for SHERPA, DIPHOX + GAMMA2MC, and RESBOS, and the MSTW2008 [37] NNLO PDF set for 2γ NNLO. The DIPHOX and GAMMA2MC theoretical uncertainties are computed in the following way: the factorization and renormalization scales in GAMMA2MC are varied independently up and down by a factor of two around $m_{\gamma\gamma}$ (configurations where one scale has a factor of four with respect to the other one are forbidden). In DIPHOX, the factorization, renormalization and fragmentation scales are varied in the same way. In RESBOS, the factorization and renormalization

scales are varied simultaneously by a factor of two. The maximum and minimum values in each bin are used to define the uncertainty. In DIPHOX, GAMMA2MC, and RESBOS, the 52 CT10 eigenvector sets of PDFs are used to build the PDF uncertainty envelope, also considering the uncertainty in the strong coupling constant α_S , determined according to the CT10 α_S PDF set. In 2γ NNLO, a simplified and less computationally intensive estimate of the renormalization and factorization scale uncertainties is performed by varying these scales simultaneously by a factor of two up and down around $m_{\gamma\gamma}$; no PDF uncertainty is computed. The same procedure is used in SHERPA, using the internal METS scale, where scales are defined as the lowest invariant mass or negative virtuality in the core $2 \rightarrow 2$ configuration clustered using a k_T -type algorithm.

The total cross section measured in data for the phase space defined above is:

$$\sigma = 17.2 \pm 0.2(\text{stat.}) \pm 1.9(\text{sys.}) \pm 0.4(\text{lum.}) \text{ pb,}$$

Fig. 8 The comparisons of the differential cross section between data and the SHERPA, DIPHOX + GAMMA2MC, RESBOS, and 2γ NNLO predictions for $\Delta\phi_{\gamma\gamma}$. Black dots correspond to data with error bars including all statistical and systematic uncertainties. Only the scale uncertainty is included for the SHERPA prediction. Scale, PDF and α_S uncertainties are included for DIPHOX + GAMMA2MC and RESBOS. Only statistical and scale uncertainties are included for the 2γ NNLO prediction



compared with

$$\begin{aligned}
 \sigma_{\text{NNLO}}(2\gamma\text{NNLO}) &= 16.2^{+1.5}_{-1.3} \text{ (scale) pb,} \\
 \sigma_{\text{NLO}}(\text{DIPHOX} + \text{GAMMA2MC}) &= 12.8^{+1.6}_{-1.5} \text{ (scale)}^{+0.6}_{-0.8} \text{ (pdf}+\alpha_S) \text{ pb,} \\
 \sigma_{\text{NLO}}(\text{RESBOS}) &= 14.9^{+2.2}_{-1.7} \text{ (scale)} \pm 0.6 \text{ (pdf}+\alpha_S) \text{ pb,} \\
 \sigma_{\text{LO}}(\text{SHERPA}) &= 13.8^{+2.8}_{-1.6} \text{ (scale) pb.} \quad (4)
 \end{aligned}$$

Figures 6, 7, 8 and 9 show the comparisons of the differential cross section between data and the SHERPA, DIPHOX + GAMMA2MC, RESBOS, and 2γ NNLO predictions for the four observables.

The NLO predictions of DIPHOX + GAMMA2MC are known to underestimate the data [11], because of the missing higher-order contributions. Apart from an overall normalization factor, the phase space regions where the disagreement is the largest are at low $m_{\gamma\gamma}$, low $\Delta\phi_{\gamma\gamma}$. The RESBOS generator shows a similar trend, with a cross section closer to the data than DIPHOX + GAMMA2MC; its prediction is improved at high $\Delta\phi_{\gamma\gamma}$ due to soft gluon resummation. With higher-order diagrams included, 2γ NNLO shows an improvement for the

overall normalization. It also shows a better shape description, especially at low $\Delta\phi_{\gamma\gamma}$, but it still underestimates the data in the same region. SHERPA generally reproduces rather well the shape of the data, to a similar level as 2γ NNLO. One can note that 2γ NNLO and SHERPA predict the $p_T^{\gamma\gamma}$ shoulder near $E_T^{\gamma 1} + E_T^{\gamma 2} \sim 65$ GeV observed in the data. This is expected since SHERPA includes up to three extra jets at the matrix element level.

9 Summary

A measurement of differential cross sections for the production of a pair of isolated photons in pp collisions at $\sqrt{s} = 7$ TeV has been presented. The data sample corresponds to an integrated luminosity of 5.0 fb^{-1} recorded in 2011 with the CMS detector. To enhance the sensitivity to higher-order diagrams, this measurement covers a phase space defined by an asymmetric E_T selection by requiring two isolated photons with E_T above 40 and 25 GeV respectively, in the pseudorapidity range $|\eta| < 2.5$, $|\eta| \notin [1.44, 1.57]$ and with an angular separation $\Delta R > 0.45$.

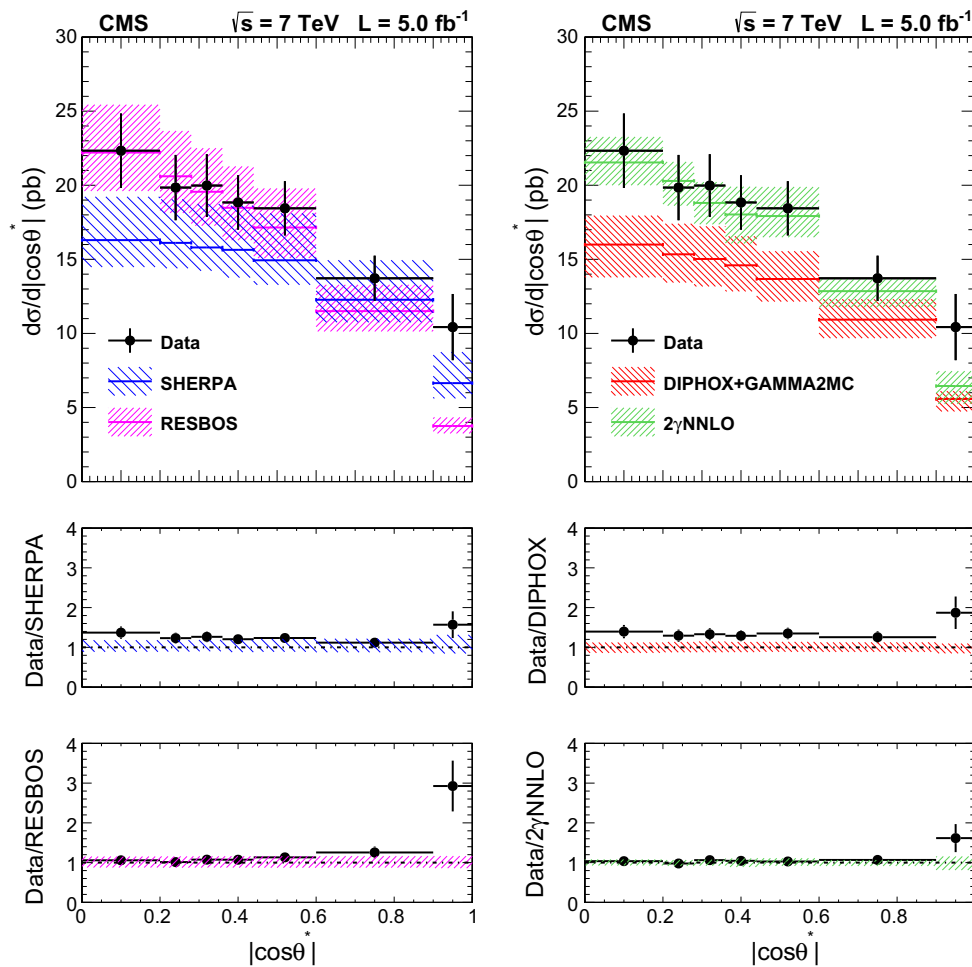


Fig. 9 The comparisons of the differential cross section between data and the SHERPA, DIPHOX + GAMMA2MC, RESBOS, and 2γ NNLO predictions for $|\cos\theta^*|$. Black dots correspond to data with error bars including all statistical and systematic uncertainties. Only the scale uncertainty

is included for the SHERPA prediction. Scale, PDF and α_S uncertainties are included for DIPHOX + GAMMA2MC and RESBOS. Only statistical and scale uncertainties are included for the 2γ NNLO prediction

A data-driven method based on the photon component of the particle flow isolation has been used to extract the prompt diphoton yield. The isolation is calculated so that the energy leakage from the photon deposit inside the isolation cone is effectively subtracted.

The measured total cross section is

$$\sigma = 17.2 \pm 0.2 \text{ (stat)} \pm 1.9 \text{ (syst)} \pm 0.4 \text{ (lumi)} \text{ pb}$$

in agreement with the 2γ NNLO prediction. The SHERPA and RESBOS predictions are compatible with the measurement within the uncertainties, while DIPHOX + GAMMA2MC underestimates the total cross section.

Differential cross sections for prompt diphoton production have been measured as a function of the diphoton invariant mass $m_{\gamma\gamma}$, the diphoton transverse momentum $p_T^{\gamma\gamma}$, the azimuthal angular separation $\Delta\phi_{\gamma\gamma}$ between the two photons, and the cosine of the polar angle θ^* in the Collins–Soper frame of the diphoton system. The 2γ NNLO and SHERPA pre-

dictions show an improved agreement in shape with the data for the kinematic distributions with respect to the DIPHOX + GAMMA2MC and RESBOS predictions, especially in the low $m_{\gamma\gamma}$, low $\Delta\phi_{\gamma\gamma}$ regions, which are the most sensitive to higher-order corrections.

Acknowledgments We congratulate our colleagues in the CERN accelerator departments for the excellent performance of the LHC and thank the technical and administrative staffs at CERN and at other CMS institutes for their contributions to the success of the CMS effort. In addition, we gratefully acknowledge the computing centres and personnel of the Worldwide LHC Computing Grid for delivering so effectively the computing infrastructure essential to our analyses. Finally, we acknowledge the enduring support for the construction and operation of the LHC and the CMS detector provided by the following funding agencies: BMFWF and FWF (Austria); FNRS and FWO (Belgium); CNPq, CAPES, FAPERJ, and FAPESP (Brazil); MES (Bulgaria); CERN; CAS, MoST, and NSFC (China); COLCIENCIAS (Colombia); MSES and CSF (Croatia); RPF (Cyprus); MoER, ERC IUT and ERDF (Estonia); Academy of Finland, MEC, and HIP (Finland); CEA and CNRS/IN2P3 (France); BMBF, DFG, and HGF (Germany); GSRT (Greece); OTKA

and NIH (Hungary); DAE and DST (India); IPM (Iran); SFI (Ireland); INFN (Italy); NRF and WCU (Republic of Korea); LAS (Lithuania); MOE and UM (Malaysia); CINVESTAV, CONACYT, SEP, and UASLP-FAI (Mexico); MBIE (New Zealand); PAEC (Pakistan); MSHE and NSC (Poland); FCT (Portugal); JINR (Dubna); MON, RosAtom, RAS and RFBR (Russia); MESTD (Serbia); SEIDI and CPAN (Spain); Swiss Funding Agencies (Switzerland); MST (Taipei); ThEPCenter, IPST, STAR and NSTDA (Thailand); TUBITAK and TAEK (Turkey); NASU and SFFR (Ukraine); STFC (United Kingdom); DOE and NSF (USA). Individuals have received support from the Marie-Curie programme and the European Research Council and EPLANET (European Union); the Leventis Foundation; the A. P. Sloan Foundation; the Alexander von Humboldt Foundation; the Belgian Federal Science Policy Office; the Fonds pour la Formation à la Recherche dans l'Industrie et dans l'Agriculture (FRIA-Belgium); the Agentschap voor Innovatie door Wetenschap en Technologie (IWT-Belgium); the Ministry of Education, Youth and Sports (MEYS) of the Czech Republic; the Council of Science and Industrial Research, India; the Compagnia di San Paolo (Torino); and the Thalís and Aristeia programmes cofinanced by EU-ESF and the Greek NSRF.

Open Access This article is distributed under the terms of the Creative Commons Attribution License which permits any use, distribution, and reproduction in any medium, provided the original author(s) and the source are credited.

Funded by SCOAP³ / License Version CC BY 4.0.

Appendix: Cross section tables

The numerical values of the cross sections for each bin of the diphoton invariant mass $m_{\gamma\gamma}$, the diphoton transverse momentum $p_T^{\gamma\gamma}$, the azimuthal angle difference $\Delta\phi_{\gamma\gamma}$ between the two photons, and the cosine of the polar angle θ^* in the Collins–Soper frame of the diphoton pair are presented in Tables 4, 5, 6, and 7.

Table 4 Values of $d\sigma/dm_{\gamma\gamma}$ (pb/GeV) for the data, SHERPA, DIPHOX +GAMMA2MC, RESBOS and 2 γ NNLO predictions

$m_{\gamma\gamma}$ (GeV)	$d\sigma/dm_{\gamma\gamma}$ (pb/GeV)				
	Data	SHERPA	DIPHOX +GAMMA2MC	RESBOS	2 γ NNLO
0–40	0.0088 ±25 % (tot.)	0.0052 +42% (scale) -22% (scale)	0.0041 +29% -17% (scale) +8.0% -6.8% (pdf)	0.0052 +8.4% -6.1% (scale) ±17% (pdf+ α_s)	0.0075 +23% -27% (scale) ±6.1% (stat.)
40–60	0.035 ±11 % (tot.)	0.021 +37% (scale) -20% (scale)	0.012 +19% -16% (scale) +3.8% -6.2% (pdf)	0.012 +10% -7.6% (scale) ±6.7% (pdf+ α_s)	0.024 +18% -19% (scale) ±3.5% (stat.)
60–70	0.097 ±15 % (tot.)	0.071 +23% (scale) -15% (scale)	0.047 +15% -14% (scale) +4.7% -3.8% (pdf)	0.058 +6.5% -6.3% (scale) ±3.8% (pdf+ α_s)	0.072 +4.3% -6.5% (scale) ±3.5 % (stat.)
70–75	0.187 ±17 % (tot.)	0.144 +20% (scale) -9.1% (scale)	0.119 +17% -12% (scale) +6.1% -1.9% (pdf)	0.151 +6.9% -5.5% (scale) ±4.1 % (pdf+ α_s)	0.151 +3.8% -4.2% (scale) ±2.3 % (stat.)
75–80	0.256 ±12 % (tot.)	0.183 +17% (scale) -8.8% (scale)	0.179 +18% -13% (scale) +2.1% -4.5% (pdf)	0.210 +7.7% -7.1% (scale) ±4.1 % (pdf+ α_s)	0.195 +5.0% -6.7% (scale) ±1.9 % (stat.)
80–85	0.275 ±12 % (tot.)	0.204 +14% (scale) -7.1% (scale)	0.223 +14% -12% (scale) +0.2% -7.7% (pdf)	0.239 +12% -10% (scale) ±4.1 % (pdf+ α_s)	0.237 +5.1% -1.2% (scale) ±5.4 % (stat.)
85–90	0.251 ±12 % (tot.)	0.198 +15% (scale) -9.5% (scale)	0.205 +11% -11% (scale) +1.7% -4.4% (pdf)	0.230 +14% -11% (scale) ±3.9 % (pdf+ α_s)	0.257 +14% -9.6% (scale) ±2.8 % (stat.)
90–95	0.224 ±11 % (tot.)	0.183 +14% (scale) -10% (scale)	0.184 +12% -9.2% (scale) +2.8% -3.1% (pdf)	0.217 +15% -11% (scale) ±3.7 % (pdf+ α_s)	0.238 +14% -7.2% (scale) ±4.2 % (stat.)
95–100	0.197 ±11 % (tot.)	0.164 +18% (scale) -8.8% (scale)	0.169 +9.3% -11% (scale) +0.4% -5.6% (pdf)	0.192 +15% -11% (scale) ±4.3 % (pdf+ α_s)	0.199 +6.0% -8.0% (scale) ±4.7 % (stat.)
100–110	0.169 ±9.4 % (tot.)	0.139 +16% (scale) -11% (scale)	0.137 +9.5% -8.5% (scale) +2.1% -3.5% (pdf)	0.159 +16% -11% (scale) ±4.1 % (pdf+ α_s)	0.173 +10% -5.7% (scale) ±3.6 % (stat.)
110–120	0.131 ±9.1 % (tot.)	0.109 +17% (scale) -11% (scale)	0.103 +9.1% -9.0% (scale) +4.69% -3.1% (pdf)	0.122 +17% -12% (scale) ±3.6 % (pdf+ α_s)	0.128 +5.0% -3.9% (scale) ±4.7 % (stat.)
120–150	0.075 ±10 % (tot.)	0.068 +20% (scale) -12% (scale)	0.064 +8.8% -8.7% (scale) +3.2% -4.7% (pdf)	0.075 +17% -12% (scale) ±3.6 % (pdf+ α_s)	0.083 +3.4% -5.9% (scale) ± 4.6 % (stat.)

Table 4 continued

$m_{\gamma\gamma}$ (GeV)	$d\sigma/dm_{\gamma\gamma}$ (pb/GeV)				
	Data	SHERPA	DIPHOX +GAMMA2MC	RESBOS	2γ NNLO
150–250	0.022 ±10 % (tot.)	0.020 +26% -14% (scale)	0.018 +10% -9.8% (scale) +6.8% -8.3% (pdf)	0.021 +18% -13% (scale) ±3.6 % (pdf+ α_s)	0.023 +3.3% -4.0% (scale) ±3.2 % (stat.)
250–400	0.0035 ±17 % (tot.)	0.0030 +33% -17% (scale)	0.0024 +18% -21% (scale) +19% -24% (pdf)	0.0029 +18% -16% (scale) ±3.8 % (pdf+ α_s)	0.0036 +16% -10% (scale) ±7.2 % (stat.)
400–800	0.0003 ±25 % (tot.)	0.0003 +49% -21% (scale)	0.0002 +68% -71% (scale) +69% -75% (pdf)	0.0002 +21% -17% (scale) ±4.6 % (pdf+ α_s)	0.0003 +21% -25% (scale) ±25 % (stat.)

Table 5 Values of $d\sigma/dp_T^{\gamma\gamma}$ (pb/GeV) for the data, SHERPA, DIPHOX +GAMMA2MC, RESBOS and 2γ NNLO predictions

$p_T^{\gamma\gamma}$ (GeV)	$d\sigma/dp_T^{\gamma\gamma}$ (pb/GeV)				
	Data	SHERPA	DIPHOX +GAMMA2MC	RESBOS	2γ NNLO
0–6	0.302 ±7.2 % (tot.)	0.187 +2.8% -3.0% (scale)	0.230 +17% -13% (scale) +8.3% -2.0% (pdf)	0.343 +51% -37% (scale) ±4.7 % (pdf+ α_s)	0.551 +7.0% -13% (scale) ±1.9 % (stat.)
6–10	0.458 ±8.0 % (tot.)	0.288 +3.4% -0.7% (scale)	0.528 +18% -14% (scale) +1.9% -2.4% (pdf)	0.421 +14% -10% (scale) ±4.7 % (pdf+ α_s)	0.404 +7.1% -1.3% (scale) ±4.8 % (stat.)
10–12	0.466 ±8.5 % (tot.)	0.295 +10% -2.4% (scale)	0.387 +18% -12% (scale) +2.5% -1.5% (pdf)	0.419 +10% -8.3% (scale) ±4.4 % (pdf+ α_s)	0.353 +3.8% -2.6% (scale) ±2.1 % (stat.)
12–14	0.451 ±12 % (tot.)	0.310 +8.2% -5.8% (scale)	0.352 +16% -14% (scale) +1.9% -2.1% (pdf)	0.419 +9.0% -7.2% (scale) ±3.9 % (pdf+ α_s)	0.335 +6.3% -10% (scale) ±2.6 % (stat.)
14–16	0.430 ±15 % (tot.)	0.314 +14% -5.6% (scale)	0.329 +15% -13% (scale) +0.9% -3.6% (pdf)	0.417 +8.1% -6.8% (scale) ±4.2 % (pdf+ α_s)	0.338 +6.6% -9.5% (scale) ±2.9 % (stat.)
16–18	0.390 ±15 % (tot.)	0.314 +13% -8.7% (scale)	0.293 +17% -12% (scale) +1.6% -2.0% (pdf)	0.394 +7.4% -5.5% (scale) ±4.0 % (pdf+ α_s)	0.324 +3.3% -3.4% (scale) ±4.3 % (stat.)
18–20	0.354 ±17 % (tot.)	0.298 +15% -11% (scale)	0.254 +18% -10% (scale) +3.0% -0.8% (pdf)	0.354 +7.3% -5.1% (scale) ±4.4 % (pdf+ α_s)	0.307 +5.7% -5.0% (scale) ±5.5 % (stat.)
20–22	0.336 ±16 % (tot.)	0.277 +16% -10% (scale)	0.226 +16% -12% (scale) +1.7% -2.5% (pdf)	0.320 +5.4% -6.3% (scale) ±3.3 % (pdf+ α_s)	0.270 +5.4% -3.4% (scale) ±4.5 % (stat.)
22–24	0.289 ±14 % (tot.)	0.255 +20% -12% (scale)	0.201 +14% -13% (scale) +1.2% -3.2% (pdf)	0.278 +9.3% -5.3% (scale) ±3.8 % (pdf+ α_s)	0.268 +18% -11% (scale) ±3.3 % (stat.)
24–28	0.245 ±14 % (tot.)	0.230 +19% -12% (scale)	0.165 +15% -10% (scale) +3.3% -2.0% (pdf)	0.239 +5.9% -5.4% (scale) ±3.9 % (pdf+ α_s)	0.223 +8.2% -9.3% (scale) ±2.7 % (stat.)
28–34	0.182 ±15 % (tot.)	0.185 +24% -15% (scale)	0.125 +14% -12% (scale) +2.2% -2.7% (pdf)	0.181 +7.0% -5.8% (scale) ±3.7 % (pdf+ α_s)	0.178 +7.4% -6.4% (scale) ±2.8 % (stat.)
34–40	0.152 ±12 % (tot.)	0.147 +26% -15% (scale)	0.093 +13% -11% (scale) +1.9% -2.8% (pdf)	0.132 +7.0% -5.2% (scale) ±3.5 % (pdf+ α_s)	0.136 +3.5% -2.1% (scale) ±3.2 % (stat.)
40–50	0.120 ±12 % (tot.)	0.114 +28% -18% (scale)	0.065 +14% -11% (scale) +3.1% -2.7% (pdf)	0.090 +8.2% -6.7% (scale) ±2.8 % (pdf+ α_s)	0.107 +14% -10% (scale) ±1.7 % (stat.)
50–60	0.099 ±11 % (tot.)	0.084 +34% -19% (scale)	0.046 +16% -11% (scale) +2.5% -3.9% (pdf)	0.060 +7.8% -6.7% (scale) ±2.4 % (pdf+ α_s)	0.077 +9.6% -9.1% (scale) ±2.9 % (stat.)
60–70	0.088 ±12 % (tot.)	0.067 +35% -21% (scale)	0.037 +14% -12% (scale) +3.4% -4.4% (pdf)	0.043 +9.8% -7.5% (scale) ±3.2 % (pdf+ α_s)	0.066 +12% -13% (scale) ±4.4 % (stat.)

Table 5 continued

$p_T^{\gamma\gamma}$ (GeV)	$d\sigma/dp_T^{\gamma\gamma}$ (pb/GeV)				
	Data	SHERPA	DIPHOX +GAMMA2MC	RESBOS	2 γ NNLO
70–80	0.070 ± 14 %(tot.)	0.054 +36% -20% (scale)	0.030 +16% -14% (scale) +4.1% -4.5% (pdf)	0.034 +9.1% -7.5% (scale) ± 5.3 %(pdf+ α_s)	0.057 +25% -19% (scale) ± 4.0 %(stat.)
80–90	0.051 ± 12 %(tot.)	0.038 +38% -22% (scale)	0.021 +17% -14% (scale) +4.7% -4.9% (pdf)	0.027 +11% -9.0% (scale) ± 3.5 %(pdf+ α_s)	0.041 +16% -18% (scale) ± 5.8 %(stat.)
90–100	0.033 ± 14 %(tot.)	0.025 +44% -21% (scale)	0.014 +22% -13% (scale) +9.1% -3.6% (pdf)	0.016 +12% -6.9% (scale) ± 4.4 %(pdf+ α_s)	0.030 +2.3% -4.0% (scale) ± 7.0 %(stat.)
100–120	0.018 ± 12 %(tot.)	0.015 +44% -24% (scale)	0.008 +21% -14% (scale) +9.3% -6.2% (pdf)	0.010 +9.2% -10% (scale) ± 6.2 %(pdf+ α_s)	0.017 +8.4% -9.1% (scale) ± 7.6 %(stat.)
120–200	0.0044 ± 13 %(tot.)	0.0039 +48% -26% (scale)	0.0023 +24% -17% (scale) +14% -13% (pdf)	0.0032 +12% -9.0% (scale) ± 7.1 %(pdf+ α_s)	0.0043 +18% -8.0% (scale) ± 14 %(stat.)

Table 6 Values of $d\sigma/d\Delta\phi_{\gamma\gamma}$ (pb/rad) for the data, SHERPA, DIPHOX +GAMMA2MC, RESBOS and 2 γ NNLO predictions

$\Delta\phi_{\gamma\gamma}$ (rad)	$d\sigma/d\Delta\phi_{\gamma\gamma}$ (pb/rad)				
	Data	SHERPA	DIPHOX +GAMMA2MC	RESBOS	2 γ NNLO
(0.00–0.20) π	0.92 ± 19 %(tot.)	0.58 +42% -22% (scale)	0.36 +24% -16% (scale) +7.2% -6.9% (pdf)	0.41 +9.9% -7.6% (scale) ± 15 %(pdf+ α_s)	0.71 +17% -18% (scale) ± 3.5 %(stat.)
(0.20–0.40) π	1.42 ± 12 %(tot.)	0.85 +43% -24% (scale)	0.45 +21% -14% (scale) +7.0% -5.3% (pdf)	0.44 +11% -9% (scale) ± 3.1 %(pdf+ α_s)	0.98 +12% -18% (scale) ± 3.0 %(stat.)
(0.40–0.60) π	2.06 ± 11 %(tot.)	1.50 +39% -20% (scale)	0.68 +15% -14% (scale) +3.6% -6.0% (pdf)	0.76 +9.8% -7.4% (scale) ± 2.8 %(pdf+ α_s)	1.38 +12% -12% (scale) ± 2.3 %(stat.)
(0.60–0.70) π	3.42 ± 10 %(tot.)	2.69 +31% -19% (scale)	1.21 +17% -11% (scale) +4.1% -3.3% (pdf)	1.60 +8.5% -6.5% (scale) ± 3.0 %(pdf+ α_s)	2.33 +10% -10% (scale) ± 2.6 %(stat.)
(0.70–0.80) π	5.64 ± 9.8 %(tot.)	4.43 +29% -17% (scale)	2.32 +15% -11% (scale) +2.5% -2.9% (pdf)	3.21 +7.4% -6.1% (scale) ± 3.0 %(pdf+ α_s)	4.02 +8.1% -8.1% (scale) ± 1.8 %(stat.)
(0.80–0.84) π	8.95 ± 10 %(tot.)	6.85 +24% -15% (scale)	4.06 +15% -12% (scale) +2.1% -2.5% (pdf)	5.75 +7.4% -6.1% (scale) ± 3.3 %(pdf+ α_s)	7.01 +19% -10% (scale) ± 3.2 %(stat.)
(0.84–0.88) π	10.9 ± 11 %(tot.)	9.3 +20% -15% (scale)	6.3 +15% -11% (scale) +2.1% -2.3% (pdf)	8.56 +7.8% -5.9% (scale) ± 3.5 %(pdf+ α_s)	9.41 +9.0% -11% (scale) ± 3.7 %(stat.)
(0.88–0.90) π	14.4 ± 11 %(tot.)	12.0 +19% -13% (scale)	9.1 +15% -12% (scale) +4.3% -1.7% (pdf)	12.0 +7.6% -5.9% (scale) ± 3.6 %(pdf+ α_s)	12.2 +7.7% -11% (scale) ± 4.2 %(stat.)
(0.90–0.92) π	16.9 ± 11 %(tot.)	14.0 +18% -11% (scale)	12.3 +14% -12% (scale) +2.8% -2.3% (pdf)	15.3 +8.2% -6.6% (scale) ± 3.5 %(pdf+ α_s)	14.1 +8.3% -3.8% (scale) ± 11 %(stat.)
(0.92–0.94) π	21.4 ± 11 %(tot.)	17.1 +16% -9.0% (scale)	17.0 +19% -12% (scale) +3.6% -1.8% (pdf)	20.8 +8.6% -6.9% (scale) ± 3.9 %(pdf+ α_s)	18.7 +7.4% -2.4% (scale) ± 5.9 %(stat.)
(0.94–0.96) π	24.9 ± 11 %(tot.)	20.7 +14% -6.1% (scale)	25.0 +16% -12% (scale) +6.2% -1.7% (pdf)	28.0 +9.8% -7.6% (scale) ± 3.8 %(pdf+ α_s)	23.4 +8.2% -2.3% (scale) ± 3.1 %(stat.)
(0.96–0.98) π	29.1 ± 12 %(tot.)	26.2 +10% -6.2% (scale)	43.3 +17% -14% (scale) +1.5% -2.1% (pdf)	38.6 +13% -10% (scale) ± 4.0 %(pdf+ α_s)	34.3 +3.2% -6.9% (scale) ± 3.1 %(stat.)
(0.98–1.00) π	38.2 ± 11 %(tot.)	32.2 +7.1% -2.3% (scale)	44.3 +7.4% -14% (scale) +0.8% -4.6% (pdf)	54.1 +32% -23% (scale) ± 4.3 %(pdf+ α_s)	54.6 +8.0% -7.3% (scale) ± 2.0 %(stat.)

Table 7 Values of $d\sigma/d|\cos\theta^*|$ (pb) for the data, SHERPA, DIPHOX +GAMMA2MC, RESBOS and 2γ NNLO predictions

$ \cos\theta^* $	$d\sigma/d \cos\theta^* $ (pb)				
	Data	SHERPA	DIPHOX +GAMMA2MC	RESBOS	2γ NNLO
0.00–0.20	22.3 ± 11 %(tot.)	16.0 $+18\%$ -11% (scale)	16.0 $+11\%$ -11% (scale) $+2.6\%$ -6.5% (pdf)	21.1 $+14\%$ -11% (scale) ± 3.7 % (pdf+ α_s)	21.5 $+6.5\%$ -5.4% (scale) ± 2.0 % (stat.)
0.20–0.28	19.8 ± 11 %(tot.)	16.1 $+18\%$ -10% (scale)	15.3 $+11\%$ -10% (scale) $+5.0\%$ -4.4% (pdf)	19.6 $+14\%$ -11% (scale) ± 3.8 % (pdf+ α_s)	20.3 $+3.7\%$ -6.4% (scale) ± 2.9 % (stat.)
0.28–0.36	20.0 ± 10 %(tot.)	15.8 $+19\%$ -10% (scale)	15.0 $+13\%$ -10% (scale) $+4.4\%$ -5.3% (pdf)	18.6 $+14\%$ -11% (scale) ± 3.8 % (pdf+ α_s)	18.8 $+5.5\%$ -5.7% (scale) ± 2.9 % (stat.)
0.36–0.44	18.8 ± 9.7 %(tot.)	15.6 $+19\%$ -12% (scale)	14.6 $+11\%$ -10% (scale) $+4.8\%$ -4.3% (pdf)	17.6 $+14\%$ -11% (scale) ± 3.8 % (pdf+ α_s)	18.0 $+9.0\%$ -9.5% (scale) ± 3.1 % (stat.)
0.44–0.60	18.4 ± 9.9 %(tot.)	14.9 $+21\%$ -11% (scale)	13.7 $+11\%$ -9.3% (scale) $+5.4\%$ -4.5% (pdf)	16.3 $+15\%$ -11% (scale) ± 3.7 % (pdf+ α_s)	17.9 $+9.9\%$ -6.4% (scale) ± 2.1 % (stat.)
0.60–0.90	13.7 ± 11 %(tot.)	12.2 $+22\%$ -12% (scale)	10.9 $+11\%$ -9.2% (scale) $+4.3\%$ -5.4% (pdf)	10.9 $+15\%$ -11% (scale) ± 3.7 % (pdf+ α_s)	12.9 $+3.9\%$ -6.8% (scale) ± 2.7 % (stat.)
0.90–1.00	10.4 ± 21 %(tot.)	6.7 $+32\%$ -16% (scale)	5.6 $+8.0\%$ -13% (scale) $+2.9\%$ -6.4% (pdf)	3.6 $+14\%$ -11% (scale) ± 6.2 % (pdf+ α_s)	6.5 $+13\%$ -17% (scale) ± 5.5 % (stat.)

References

- ATLAS Collaboration, Observation of a new particle in the search for the Standard Model Higgs boson with the ATLAS detector at the LHC. *Phys. Lett. B* **716**, 1 (2012). doi:[10.1016/j.physletb.2012.08.020](https://doi.org/10.1016/j.physletb.2012.08.020). arXiv:[1207.7214](https://arxiv.org/abs/1207.7214)
- CMS Collaboration, Observation of a new boson at a mass of 125 GeV with the CMS experiment at the LHC. *Phys. Lett. B* **716**, 30 (2012). doi:[10.1016/j.physletb.2012.08.021](https://doi.org/10.1016/j.physletb.2012.08.021). arXiv:[1207.7235](https://arxiv.org/abs/1207.7235)
- CMS Collaboration, Observation of a new boson with mass near 125 GeV in pp collisions at $\sqrt{s} = 7$ and 8 TeV. *J. High Energy Phys.* **06**, 081 (2013). doi:[10.1007/JHEP06\(2013\)081](https://doi.org/10.1007/JHEP06(2013)081). arXiv:[1303.4571](https://arxiv.org/abs/1303.4571)
- J.T. Ruderman, D. Shih, General neutralino NLSPs at the early LHC. *J. High Energy Phys.* **08**, 159 (2012). doi:[10.1007/JHEP08\(2012\)159](https://doi.org/10.1007/JHEP08(2012)159). arXiv:[1103.6083](https://arxiv.org/abs/1103.6083)
- N. Arkani-Hamed, S. Dimopoulos, G.R. Dvali, The hierarchy problem and new dimensions at a millimeter. *Phys. Lett. B* **429**, 263 (1998). doi:[10.1016/S0370-2693\(98\)00466-3](https://doi.org/10.1016/S0370-2693(98)00466-3). arXiv:[hep-ph/9803315](https://arxiv.org/abs/hep-ph/9803315)
- L. Randall, R. Sundrum, A large mass hierarchy from a small extra dimension. *Phys. Rev. Lett.* **83**, 3370 (1999). doi:[10.1103/PhysRevLett.83.3370](https://doi.org/10.1103/PhysRevLett.83.3370). arXiv:[hep-ph/9905221](https://arxiv.org/abs/hep-ph/9905221)
- L. Randall, R. Sundrum, An alternative to compactification. *Phys. Rev. Lett.* **83**, 4690 (1999). doi:[10.1103/PhysRevLett.83.4690](https://doi.org/10.1103/PhysRevLett.83.4690). arXiv:[hep-th/9906064](https://arxiv.org/abs/hep-th/9906064)
- CDF Collaboration, Measurement of the cross section for prompt isolated diphoton production using the full CDF Run II data sample. *Phys. Rev. Lett.* **110**, 101801 (2013). doi:[10.1103/PhysRevLett.110.101801](https://doi.org/10.1103/PhysRevLett.110.101801). arXiv:[1212.4204](https://arxiv.org/abs/1212.4204)
- D0 Collaboration, Measurement of the differential cross sections for isolated direct photon pair production in $p\bar{p}$ collisions at $\sqrt{s} = 1.96$ TeV. *Phys. Lett. B* **725**, 6 (2013). doi:[10.1016/j.physletb.2013.06.036](https://doi.org/10.1016/j.physletb.2013.06.036). arXiv:[1301.4536](https://arxiv.org/abs/1301.4536)
- ATLAS Collaboration, Measurement of isolated-photon pair production in pp collisions at $\sqrt{s} = 7$ TeV with the ATLAS detector. *J. High Energy Phys.* **01**, 086 (2013). doi:[10.1007/JHEP01\(2013\)086](https://doi.org/10.1007/JHEP01(2013)086). arXiv:[1211.1913](https://arxiv.org/abs/1211.1913)
- CMS Collaboration, Measurement of the production cross section for pairs of isolated photons in pp collisions at $\sqrt{s} = 7$ TeV. *J. High Energy Phys.* **01**, 133 (2012). doi:[10.1007/JHEP01\(2012\)133](https://doi.org/10.1007/JHEP01(2012)133). arXiv:[1110.6461](https://arxiv.org/abs/1110.6461)
- CMS Collaboration, Measurement of the isolated prompt photon production cross section in pp collisions at $\sqrt{s} = 7$ TeV. *Phys. Rev. Lett.* **106**, 082001 (2011). doi:[10.1103/PhysRevLett.106.082001](https://doi.org/10.1103/PhysRevLett.106.082001). arXiv:[1012.0799](https://arxiv.org/abs/1012.0799)
- CMS Collaboration, Measurement of the differential cross section for isolated prompt photon production in pp collisions at 7 TeV. *Phys. Rev. D* **84**, 052011 (2011). doi:[10.1103/PhysRevD.84.052011](https://doi.org/10.1103/PhysRevD.84.052011). arXiv:[1108.2044](https://arxiv.org/abs/1108.2044)
- CMS Collaboration, Commissioning of the particle-flow reconstruction in minimum-bias and jet events from pp collisions at 7 TeV. CMS Physics Analysis Summary. *CMS-PAS-PFT-10-002* (2010)
- CMS Collaboration, The CMS experiment at the CERN LHC. *J. Inst.* **3**, S08004 (2008). doi:[10.1088/1748-0221/3/08/S08004](https://doi.org/10.1088/1748-0221/3/08/S08004)
- CMS Collaborations, Measurement of the inclusive W and Z production cross sections in pp collisions at $\sqrt{s} = 7$ TeV. *J. High Energy Phys.* **10**, 132 (2011). doi:[10.1007/JHEP10\(2011\)132](https://doi.org/10.1007/JHEP10(2011)132). arXiv:[1107.4789](https://arxiv.org/abs/1107.4789)
- J. Alwall et al., MadGraph 5: going beyond. *J. High Energy Phys.* **06**, 128 (2011). doi:[10.1007/JHEP06\(2011\)128](https://doi.org/10.1007/JHEP06(2011)128). arXiv:[1106.0522](https://arxiv.org/abs/1106.0522)
- T. Sjöstrand, S. Mrenna, P.Z. Skands, PYTHIA 6.4 physics and manual. *J. High Energy Phys.* **05**, 026 (2006). doi:[10.1088/1126-6708/2006/05/026](https://doi.org/10.1088/1126-6708/2006/05/026). arXiv:[hep-ph/0603175](https://arxiv.org/abs/hep-ph/0603175)
- J. Pumplin et al., New generation of parton distributions with uncertainties from global QCD analysis. *J. High Energy Phys.* **07**, 012 (2002). doi:[10.1088/1126-6708/2002/07/012](https://doi.org/10.1088/1126-6708/2002/07/012). arXiv:[hep-ph/0201195](https://arxiv.org/abs/hep-ph/0201195)
- CMS Collaboration, Measurement of the underlying event activity at the LHC with $\sqrt{s} = 7$ TeV and comparison with $\sqrt{s} = 0.9$ TeV. *J. High Energy Phys.* **09**, 109 (2011). doi:[10.1007/JHEP09\(2011\)109](https://doi.org/10.1007/JHEP09(2011)109). arXiv:[1107.0330](https://arxiv.org/abs/1107.0330)

21. GEANT4 Collaboration, GEANT4—a simulation toolkit. Nucl. Instrum. Methods A **506**, 250 (2003). doi:[10.1016/S0168-9002\(03\)01368-8](https://doi.org/10.1016/S0168-9002(03)01368-8)
22. CMS Collaboration, Energy calibration and resolution of the CMS electromagnetic calorimeter in pp collisions at $\sqrt{s} = 7$ TeV. J. Inst. **8**, P09009 (2013). doi:[10.1088/1748-0221/8/09/P09009](https://doi.org/10.1088/1748-0221/8/09/P09009). arXiv:[1306.2016](https://arxiv.org/abs/1306.2016)
23. W. Adam, R. Frühwirth, A. Strandlie, T. Todorov, Reconstruction of electrons with the Gaussian-sum filter in the CMS tracker at the LHC. J. Phys. G **31**, N9 (2005). doi:[10.1088/0954-3889/31/9/N01](https://doi.org/10.1088/0954-3889/31/9/N01)
24. J.C. Collins, D.E. Soper, Angular distribution of dileptons in high-energy hadron collisions. Phys. Rev. D **16**, 2219 (1977). doi:[10.1103/PhysRevD.16.2219](https://doi.org/10.1103/PhysRevD.16.2219)
25. M. Cacciari, G.P. Salam, Pileup subtraction using jet areas. Phys. Lett. B **659**, 119 (2008). doi:[10.1016/j.physletb.2007.09.077](https://doi.org/10.1016/j.physletb.2007.09.077). arXiv:[0707.1378](https://arxiv.org/abs/0707.1378)
26. G. D'Agostini, A multidimensional unfolding method based on Bayes theorem. Nucl. Instrum. Methods A **372**, 46 (1996). doi:[10.1016/0168-9002\(95\)00274-X](https://doi.org/10.1016/0168-9002(95)00274-X)
27. T. Auye, in *Proceedings of the PHYSTAT 2011 Workshop on Statistical Issues Related to Discovery Claims in Search Experiments and Unfolding*. Unfolding Algorithms and Tests Using RooUnfold (2011), p. 313. doi:[10.5170/CERN-2011-006](https://doi.org/10.5170/CERN-2011-006)
28. CMS Collaboration, Absolute calibration of the luminosity measurement at CMS: winter 2012 update. CMS Physics Analysis Summary. CMS-PAS-SMP-12-008 (2012)
29. T. Gleisberg et al., Event generation with SHERPA 1.1. J. High Energy Phys. **02**, 007 (2009). doi:[10.1088/1126-6708/2009/02/007](https://doi.org/10.1088/1126-6708/2009/02/007). arXiv:[0811.4622](https://arxiv.org/abs/0811.4622)
30. T. Binoth, J.P. Guillet, E. Pilon, M. Werlen, A full next-to-leading order study of direct photon pair production in hadronic collisions. Eur. Phys. J. C **16**, 311 (2000). doi:[10.1007/s100520050024](https://doi.org/10.1007/s100520050024). arXiv:[hep-ph/9911340](https://arxiv.org/abs/hep-ph/9911340)
31. Z. Bern, L.J. Dixon, C. Schmidt, Isolating a light Higgs boson from the diphoton background at the CERN LHC. Phys. Rev. D **66**, 074018 (2002). doi:[10.1103/PhysRevD.66.074018](https://doi.org/10.1103/PhysRevD.66.074018). arXiv:[hep-ph/0206194](https://arxiv.org/abs/hep-ph/0206194)
32. C. Balazs, E.L. Berger, S. Mrenna, C.P. Yuan, Photon pair production with soft gluon resummation in hadronic interactions. Phys. Rev. D **57**, 6934 (1998). doi:[10.1103/PhysRevD.57.6934](https://doi.org/10.1103/PhysRevD.57.6934)
33. C. Balázs, E.L. Berger, P.M. Nadolsky, C.-P. Yuan, Calculation of prompt diphoton production cross-sections at Tevatron and LHC energies. Phys. Rev. D **76**, 013009 (2007). doi:[10.1103/PhysRevD.76.013009](https://doi.org/10.1103/PhysRevD.76.013009)
34. S. Catani et al., Diphoton production at hadron colliders: a fully-differential QCD calculation at NNLO. Phys. Rev. Lett. **108**, 072001 (2012). doi:[10.1103/PhysRevLett.108.072001](https://doi.org/10.1103/PhysRevLett.108.072001). arXiv:[1110.2375](https://arxiv.org/abs/1110.2375)
35. S. Frixione, Isolated photons in perturbative QCD. Phys. Lett. B **429**, 369 (1998). doi:[10.1016/S0370-2693\(98\)00454-7](https://doi.org/10.1016/S0370-2693(98)00454-7). arXiv:[hep-ph/9801442](https://arxiv.org/abs/hep-ph/9801442)
36. H.-L. Lai et al., New parton distributions for collider physics. Phys. Rev. D **82**, 074024 (2010). doi:[10.1103/PhysRevD.82.074024](https://doi.org/10.1103/PhysRevD.82.074024). arXiv:[1007.2241](https://arxiv.org/abs/1007.2241)
37. A.D. Martin, W.J. Stirling, R.S. Thorne, G. Watt, Parton distributions for the LHC. Eur. Phys. J. C **63**, 189 (2009). doi:[10.1140/epjc/s10052-009-1072-5](https://doi.org/10.1140/epjc/s10052-009-1072-5). arXiv:[0901.0002](https://arxiv.org/abs/0901.0002)

CMS Collaboration

Yerevan Physics Institute, Yerevan, Armenia

S. Chatrchyan, V. Khachatryan, A. M. Sirunyan, A. Tumasyan

Institut für Hochenergiephysik der OeAW, Vienna, Austria

W. Adam, T. Bergauer, M. Dragicevic, J. Erö, C. Fabjan¹, M. Friedl, R. Frühwirth¹, V. M. Ghete, C. Hartl, N. Hörmann, J. Hrubec, M. Jeitler¹, W. Kiesenhofer, V. Knünz, M. Krammer¹, I. Krätschmer, D. Liko, I. Mikulec, D. Rabady², B. Rahbaran, H. Rohringer, R. Schöfbeck, J. Strauss, A. Taurok, W. Treberer-Treberspurg, W. Waltenberger, C.-E. Wulz¹

National Centre for Particle and High Energy Physics, Minsk, Belarus

V. Mossolov, N. Shumeiko, J. Suarez Gonzalez

Universiteit Antwerpen, Antwerp, Belgium

S. Alderweireldt, M. Bansal, S. Bansal, T. Cornelis, E. A. De Wolf, X. Janssen, A. Knutsson, S. Luyckx, S. Ochesanu, B. Roland, R. Rougny, H. Van Haevermaet, P. Van Mechelen, N. Van Remortel, A. Van Spilbeeck

Vrije Universiteit Brussel, Brussels, Belgium

F. Blekman, S. Blyweert, J. D'Hondt, N. Heracleous, A. Kalogeropoulos, J. Keaveney, T. J. Kim, S. Lowette, M. Maes, A. Olbrechts, D. Strom, S. Tavernier, W. Van Doninck, P. Van Mulders, G. P. Van Onsem, I. Vilella

Université Libre de Bruxelles, Brussels, Belgium

C. Caillol, B. Clerbaux, G. De Lentdecker, L. Favart, A. P. R. Gay, A. Léonard, P. E. Marage, A. Mohammadi, L. Perniè, T. Reis, T. Seva, L. Thomas, C. Vander Velde, P. Vanlaer, J. Wang

Ghent University, Ghent, Belgium

V. Adler, K. Beernaert, L. Benucci, A. Cimmino, S. Costantini, S. Crucy, S. Dildick, G. Garcia, B. Klein, J. Lellouch, J. McCartin, A. A. Ocampo Rios, D. Ryckbosch, S. Salva Diblen, M. Sigamani, N. Strobbe, F. Thyssen, M. Tytgat, S. Walsh, E. Yazgan, N. Zaganidis

Université Catholique de Louvain, Louvain-la-Neuve, Belgium

S. Basegmez, C. Beluffi³, G. Bruno, R. Castello, A. Caudron, L. Ceard, G. G. Da Silveira, C. Delaere, T. du Pree, D. Favart, L. Forthomme, A. Giammanco⁴, J. Hollar, P. Jez, M. Komm, V. Lemaitre, J. Liao, O. Militaru, C. Nuttens, D. Pagano, A. Pin, K. Piotrkowski, A. Popov⁵, L. Quertenmont, M. Selvaggi, M. Vidal Marono, J. M. Vizan Garcia

Université de Mons, Mons, Belgium

N. Belyi, T. Caebergs, E. Daubie, G. H. Hammad

Centro Brasileiro de Pesquisas Fisicas, Rio de Janeiro, Brazil

G. A. Alves, M. Correa Martins Junior, T. Dos Reis Martins, M. E. Pol, M. H. G. Souza

Universidade do Estado do Rio de Janeiro, Rio de Janeiro, Brazil

W. L. Aldá Júnior, W. Carvalho, J. Chinellato⁶, A. Custódio, E. M. Da Costa, D. De Jesus Damiao, C. De Oliveira Martins, S. Fonseca De Souza, H. Malbouisson, M. Malek, D. Matos Figueiredo, L. Mundim, H. Nogima, W. L. Prado Da Silva, J. Santaolalla, A. Santoro, A. Sznajder, E. J. Tonelli Manganote⁶, A. Vilela Pereira

Universidade Estadual Paulista^a, Universidade Federal do ABC^b, São Paulo, Brazil

C. A. Bernardes^b, F. A. Dias^{a,7}, T. R. Fernandez Perez Tomei^a, E. M. Gregores^b, P. G. Mercadante^b, S. F. Novaes^a, Sandra S. Padula^a

Institute for Nuclear Research and Nuclear Energy, Sofia, Bulgaria

V. Genchev², P. Iaydjiev², A. Marinov, S. Piperov, M. Rodozov, G. Sultanov, M. Vutova

University of Sofia, Sofia, Bulgaria

A. Dimitrov, I. Glushkov, R. Hadjiiska, V. Kozhuharov, L. Litov, B. Pavlov, P. Petkov

Institute of High Energy Physics, Beijing, China

J. G. Bian, G. M. Chen, H. S. Chen, M. Chen, R. Du, C. H. Jiang, D. Liang, S. Liang, X. Meng, R. Plestina⁸, J. Tao, X. Wang, Z. Wang

State Key Laboratory of Nuclear Physics and Technology, Peking University, Beijing, China

C. Asawatangtrakuldee, Y. Ban, Y. Guo, Q. Li, W. Li, S. Liu, Y. Mao, S. J. Qian, D. Wang, L. Zhang, W. Zou

Universidad de Los Andes, Bogotá, Colombia

C. Avila, L. F. Chaparro Sierra, C. Florez, J. P. Gomez, B. Gomez Moreno, J. C. Sanabria

Technical University of Split, Split, Croatia

N. Godinovic, D. Lelas, D. Polic, I. Puljak

University of Split, Split, Croatia

Z. Antunovic, M. Kovac

Institute Rudjer Boskovic, Zagreb, Croatia

V. Brigljevic, K. Kadija, J. Luetic, D. Mekterovic, S. Morovic, L. Sudic

University of Cyprus, Nicosia, Cyprus

A. Attikis, G. Mavromanolakis, J. Mousa, C. Nicolaou, F. Ptochos, P. A. Razis

Charles University, Prague, Czech Republic

M. Finger, M. Finger Jr.

Academy of Scientific Research and Technology of the Arab Republic of Egypt, Egyptian Network of High Energy Physics, Cairo, Egypt

Y. Assran⁹, S. Elgammal¹⁰, A. Ellithi Kamel¹¹, M. A. Mahmoud¹², A. Mahrous¹³, A. Radi^{10,14}

National Institute of Chemical Physics and Biophysics, Tallinn, Estonia

M. Kadastik, M. Müntel, M. Murumaa, M. Raidal, A. Tiko

Department of Physics, University of Helsinki, Helsinki, Finland

P. Eerola, G. Fedi, M. Voutilainen

Helsinki Institute of Physics, Helsinki, Finland

J. Härkönen, V. Karimäki, R. Kinnunen, M. J. Kortelainen, T. Lampén, K. Lassila-Perini, S. Lehti, T. Lindén, P. Luukka, T. Mäenpää, T. Peltola, E. Tuominen, J. Tuominiemi, E. Tuovinen, L. Wendland

Lappeenranta University of Technology, Lappeenranta, Finland

T. Tuuva

DSM/IRFU, CEA/Saclay, Gif-sur-Yvette, France

M. Besancon, F. Couderc, M. Dejjardin, D. Denegri, B. Fabbro, J. L. Faure, F. Ferri, S. Ganjour, A. Givernaud, P. Gras, G. Hamel de Monchenault, P. Jarry, E. Locci, J. Malcles, A. Nayak, J. Rander, A. Rosowsky, M. Titov

Laboratoire Leprince-Ringuet, Ecole Polytechnique, IN2P3-CNRS, Palaiseau, France

S. Baffioni, F. Beaudette, P. Busson, C. Charlot, N. Daci, T. Dahms, M. Dalchenko, L. Dobrzynski, N. Filipovic, A. Florent, R. Granier de Cassagnac, L. Mastrolorenzo, P. Miné, C. Mironov, I. N. Naranjo, M. Nguyen, C. Ochando, P. Paganini, D. Sabes, R. Salerno, J. B. Sauvan, Y. Sirois, C. Veelken, Y. Yilmaz, A. Zabi

Institut Pluridisciplinaire Hubert Curien, Université de Strasbourg, Université de Haute Alsace Mulhouse, CNRS/IN2P3, Strasbourg, France

J.-L. Agram¹⁵, J. Andrea, D. Bloch, J.-M. Brom, E. C. Chabert, C. Collard, E. Conte¹⁵, F. Drouhin¹⁵, J.-C. Fontaine¹⁵, D. Gelé, U. Goerlach, C. Goetzmann, P. Juillot, A.-C. Le Bihan, P. Van Hove

Centre de Calcul de l'Institut National de Physique Nucleaire et de Physique des Particules, CNRS/IN2P3, Villeurbanne, France

S. Gadrat

Institut de Physique Nucléaire de Lyon, Université de Lyon, Université Claude Bernard Lyon 1, CNRS-IN2P3, Villeurbanne, France

S. Beauceron, N. Beaupere, G. Boudoul, S. Brochet, C. A. Carrillo Montoya, J. Chasserat, R. Chierici, D. Contardo², P. Depasse, H. El Mamouni, J. Fan, J. Fay, S. Gascon, M. Gouzevitch, B. Ille, T. Kurca, M. Lethuillier, L. Mirabito, S. Perries, J. D. Ruiz Alvarez, L. Sgandurra, V. Sordini, M. Vander Donckt, P. Verdier, S. Viret, H. Xiao

Institute of High Energy Physics and Informatization, Tbilisi State University, Tbilisi, Georgia

Z. Tsamalaidze¹⁶

RWTH Aachen University, I. Physikalisches Institut, Aachen, Germany

C. Autermann, S. Beranek, M. Bontenackels, B. Calpas, M. Edelhoff, L. Feld, O. Hindrichs, K. Klein, A. Ostapchuk, A. Perieanu, F. Raupach, J. Sammet, S. Schael, D. Sprenger, H. Weber, B. Wittmer, V. Zhukov⁵

RWTH Aachen University, III. Physikalisches Institut A, Aachen, Germany

M. Ata, J. Caudron, E. Dietz-Laursonn, D. Duchardt, M. Erdmann, R. Fischer, A. Güth, T. Hebbeker, C. Heidemann, K. Hoepfner, D. Klingebiel, S. Knutzen, P. Kreuzer, M. Merschmeyer, A. Meyer, M. Olschewski, K. Padeken, P. Papacz, H. Reithler, S. A. Schmitz, L. Sonnenschein, D. Teyssier, S. Thüer, M. Weber

RWTH Aachen University, III. Physikalisches Institut B, Aachen, Germany

V. Cherepanov, Y. Erdogan, G. Flügge, H. Geenen, M. Geisler, W. Haj Ahmad, F. Hoehle, B. Kargoll, T. Kress, Y. Kuessel, J. Lingemann², A. Nowack, I. M. Nugent, L. Perchalla, O. Pooth, A. Stahl

Deutsches Elektronen-Synchrotron, Hamburg, Germany

I. Asin, N. Bartosik, J. Behr, W. Behrenhoff, U. Behrens, A. J. Bell, M. Bergholz¹⁷, A. Bethani, K. Borras, A. Burgmeier, A. Cakir, L. Calligaris, A. Campbell, S. Choudhury, F. Costanza, C. Diez Pardos, S. Dooling, T. Dorland, G. Eckerlin, D. Eckstein, T. Eichhorn, G. Flucke, A. Geiser, A. Grebenyuk, P. Gunnellini, S. Habib, J. Hauk, G. Hellwig, M. Hempel, D. Horton, H. Jung, M. Kasemann, P. Katsas, J. Kieseler, C. Kleinwort, M. Krämer, D. Krücker, W. Lange, J. Leonard, K. Lipka, W. Lohmann¹⁷, B. Lutz, R. Mankel, I. Marfin, I.-A. Melzer-Pellmann, A. B. Meyer, J. Mnich, A. Mussgiller, S. Naumann-Emme, O. Novgorodova, F. Nowak, E. Ntomari, H. Perrey, A. Petrukhin, D. Pitzl, R. Placakyte, A. Raspereza, P. M. Ribeiro Cipriano, C. Riedl, E. Ron, M. Ö. Sahin, J. Salfeld-Nebgen, P. Saxena, R. Schmidt¹⁷, T. Schoerner-Sadenius, M. Schröder, M. Stein, A. D. R. Vargias Trevino, R. Walsh, C. Wissing

University of Hamburg, Hamburg, Germany

M. Aldaya Martin, V. Blobel, H. Enderle, J. Erfle, E. Garutti, K. Goebel, M. Görner, M. Gosselink, J. Haller, R. S. Höing, H. Kirschenmann, R. Klanner, R. Kogler, J. Lange, T. Lapsien, T. Lenz, I. Marchesini, J. Ott, T. Peiffer, N. Pietsch, D. Rathjens, C. Sander, H. Schettler, P. Schleper, E. Schlieckau, A. Schmidt, M. Seidel, J. Sibille¹⁸, V. Sola, H. Stadie, G. Steinbrück, D. Troendle, E. Usai, L. Vanelderen

Institut für Experimentelle Kernphysik, Karlsruhe, Germany

C. Barth, C. Baus, J. Berger, C. Böser, E. Butz, T. Chwalek, W. De Boer, A. Descroix, A. Dierlamm, M. Feindt, M. Guthoff², F. Hartmann², T. Hauth², H. Held, K. H. Hoffmann, U. Husemann, I. Katkov⁵, A. Kornmayer², E. Kuznetsova, P. Lobelle Pardo, D. Martschei, M. U. Mozer, Th. Müller, M. Niegel, A. Nürnberg, O. Oberst, G. Quast, K. Rabbertz, F. Ratnikov, S. Röcker, F.-P. Schilling, G. Schott, H. J. Simonis, F. M. Stober, R. Ulrich, J. Wagner-Kuhr, S. Wayand, T. Weiler, R. Wolf, M. Zeise

Institute of Nuclear and Particle Physics (INPP), NCSR Demokritos, Aghia Paraskevi, Greece

G. Anagnostou, G. Daskalakis, T. Gerasimidis, S. Kesisoglou, A. Kyriakis, D. Loukas, A. Markou, C. Markou, A. Psallidas, I. Topsis-Giotis

University of Athens, Athens, Greece

L. Gouskos, A. Panagiotou, N. Saoulidou, E. Stiliaris

University of Ioánnina, Ioannina, Greece

X. Aslanoglou, I. Evangelou², G. Flouris, C. Foudas², J. Jones, P. Kokkas, N. Manthos, I. Papadopoulos, E. Paradas

Wigner Research Centre for Physics, Budapest, Hungary

G. Bencze², C. Hajdu, P. Hidas, D. Horvath¹⁹, F. Sikler, V. Veszpremi, G. Vesztergombi²⁰, A. J. Zsigmond

Institute of Nuclear Research ATOMKI, Debrecen, Hungary

N. Beni, S. Czellar, J. Molnar, J. Palinkas, Z. Szillasi

University of Debrecen, Debrecen, Hungary

J. Karancsi, P. Raics, Z. L. Trocsanyi, B. Ujvari

National Institute of Science Education and Research, Bhubaneswar, India

S. K. Swain

Panjab University, Chandigarh, India

S. B. Beri, V. Bhatnagar, N. Dhingra, R. Gupta, M. Kaur, M. Mittal, N. Nishu, A. Sharma, J. B. Singh

University of Delhi, Delhi, India

Ashok Kumar, Arun Kumar, S. Ahuja, A. Bhardwaj, B. C. Choudhary, A. Kumar, S. Malhotra, M. Naimuddin, K. Ranjan, V. Sharma, R. K. Shivpuri

Saha Institute of Nuclear Physics, Kolkata, India

S. Banerjee, S. Bhattacharya, K. Chatterjee, S. Dutta, B. Gomber, Sa. Jain, Sh. Jain, R. Khurana, A. Modak, S. Mukherjee, D. Roy, S. Sarkar, M. Sharan, A. P. Singh

Bhabha Atomic Research Centre, Mumbai, India

A. Abdulsalam, D. Dutta, S. Kailas, V. Kumar, A. K. Mohanty², L. M. Pant, P. Shukla, A. Topkar

Tata Institute of Fundamental Research, Mumbai, India

T. Aziz, S. Banerjee, R. M. Chatterjee, S. Dugad, S. Ganguly, S. Ghosh, M. Guchait, A. Gurtu²¹, G. Kole, S. Kumar, M. Maity²², G. Majumder, K. Mazumdar, G. B. Mohanty, B. Parida, K. Sudhakar, N. Wickramage²³

Institute for Research in Fundamental Sciences (IPM), Tehran, Iran

H. Arfaei, H. Bakhshiansohi, H. Behnamian, S. M. Etesami²⁴, A. Fahim²⁵, A. Jafari, M. Khakzad, M. Mohammadi Najafabadi, M. Naseri, S. Paktinat Mehdiabadi, B. Safarzadeh²⁶, M. Zeinali

University College Dublin, Dublin, Ireland

M. Grunewald

INFN Sezione di Bari^a, Università di Bari^b, Politecnico di Bari^c, Bari, Italy

M. Abbrescia^{a,b}, L. Barbore^{a,b}, C. Calabria^{a,b}, S. S. Chhibra^{a,b}, A. Colaleo^a, D. Creanza^{a,c}, N. De Filippis^{a,c}, M. De Palma^{a,b}, L. Fiore^a, G. Iaselli^{a,c}, G. Maggi^{a,c}, M. Maggi^a, B. Marangelli^{a,b}, S. My^{a,c}, S. Nuzzo^{a,b}, N. Pacifico^a, A. Pompili^{a,b}, G. Pugliese^{a,c}, R. Radogna^{a,b}, G. Selvaggi^{a,b}, L. Silvestris^a, G. Singh^{a,b}, R. Venditti^{a,b}, P. Verwilligen^a, G. Zito^a

INFN Sezione di Bologna^a, Università di Bologna^b, Bologna, Italy

G. Abbiendi^a, A. C. Benvenuti^a, D. Bonacorsi^{a,b}, S. Braibant-Giacomelli^{a,b}, L. Brigliadori^{a,b}, R. Campanini^{a,b}, P. Capiluppi^{a,b}, A. Castro^{a,b}, F. R. Cavallo^a, G. Codispoti^{a,b}, M. Cuffiani^{a,b}, G. M. Dallavalle^a, F. Fabbri^a, A. Fanfani^{a,b}, D. Fasanella^{a,b}, P. Giacomelli^a, C. Grandi^a, L. Guiducci^{a,b}, S. Marcellini^a, G. Masetti^a, M. Meneghelli^{a,b}, A. Montanari^a, F. L. Navarria^{a,b}, F. Odorici^a, A. Perrotta^a, F. Primavera^{a,b}, A. M. Rossi^{a,b}, T. Rovelli^{a,b}, G. P. Siroli^{a,b}, N. Tosi^{a,b}, R. Travaglini^{a,b}

INFN Sezione di Catania^a, Università di Catania^b, CSFNSM^c, Catania, Italy

S. Albergo^{a,b}, G. Cappello^a, M. Chiorboli^{a,b}, S. Costa^{a,b}, F. Giordano^{a,c,2}, R. Potenza^{a,b}, A. Tricomi^{a,b}, C. Tuve^{a,b}

INFN Sezione di Firenze^a, Università di Firenze^b, Florence, Italy

G. Barbagli^a, V. Ciulli^{a,b}, C. Civinini^a, R. D'Alessandro^{a,b}, E. Focardi^{a,b}, E. Gallo^a, S. Gozzi^{a,b}, V. Gori^{a,b}, P. Lenzi^{a,b}, M. Meschini^a, S. Paoletti^a, G. Sguazzoni^a, A. Tropiano^{a,b}

INFN Laboratori Nazionali di Frascati, Frascati, Italy

L. Benussi, S. Bianco, F. Fabbri, D. Piccolo

INFN Sezione di Genova^a, Università di Genova^b, Genoa, Italy

P. Fabbriatore^a, R. Ferretti^{a,b}, F. Ferro^a, M. Lo Vetere^{a,b}, R. Musenich^a, E. Robutti^a, S. Tosi^{a,b}

INFN Sezione di Milano-Bicocca^a, Università di Milano-Bicocca^b, Milan, Italy

M. E. Dinardo^{a,b}, S. Fiorendi^{a,b,2}, S. Gennai^a, R. Gerosa, A. Ghezzi^{a,b}, P. Govoni^{a,b}, M. T. Lucchini^{a,b,2}, S. Malvezzi^a, R. A. Manzoni^{a,b,2}, A. Martelli^{a,b,2}, B. Marzocchi, D. Menasce^a, L. Moroni^a, M. Paganoni^{a,b}, D. Pedrini^a, S. Ragazzi^{a,b}, N. Redaelli^a, T. Tabarelli de Fatis^{a,b}

INFN Sezione di Napoli^a, Università di Napoli 'Federico II'^b, Università della Basilicata (Potenza)^c, Università G. Marconi (Roma)^d, Naples, Italy

S. Buontempo^a, N. Cavallo^{a,c}, S. Di Guida^{a,d}, F. Fabozzi^{a,c}, A. O. M. Iorio^{a,b}, L. Lista^a, S. Meola^{a,d,2}, M. Merola^a, P. Paolucci^{a,2}

INFN Sezione di Padova^a, Università di Padova^b, Università di Trento (Trento)^c, Padua, Italy

P. Azzi^a, M. Bellato^a, M. Biasotto^{a,27}, D. Bisello^{a,b}, A. Branca^{a,b}, P. Checchia^a, T. Dorigo^a, U. Dosselli^a, F. Fanzago^a, M. Galanti^{a,b,2}, F. Gasparini^{a,b}, U. Gasparini^{a,b}, P. Giubilato^{a,b}, F. Gonella^a, A. Gozzelino^a, K. Kanishchev^{a,c}, S. Lacaprara^a, I. Lazzizzera^{a,c}, M. Margoni^{a,b}, A. T. Meneguzzo^{a,b}, J. Pazzini^{a,b}, N. Pozzobon^{a,b}, P. Ronchese^{a,b}, F. Simonetto^{a,b}, E. Torassa^a, M. Tosi^{a,b}, P. Zotto^{a,b}, A. Zucchetta^{a,b}, G. Zumerle^{a,b}

INFN Sezione di Pavia^a, Università di Pavia^b, Pavia, Italy

M. Gabusi^{a,b}, S. P. Ratti^{a,b}, C. Riccardi^{a,b}, P. Salvini^a, P. Vitulo^{a,b}

INFN Sezione di Perugia^a, Università di Perugia^b, Perugia, Italy

M. Biasini^{a,b}, G. M. Bilei^a, L. Fanò^{a,b}, P. Lariccia^{a,b}, G. Mantovani^{a,b}, M. Menichelli^a, F. Romeo^{a,b}, A. Saha^a, A. Santocchia^{a,b}, A. Spiezia^{a,b}

INFN Sezione di Pisa^a, Università di Pisa^b, Scuola Normale Superiore di Pisa^c, Pisa, Italy

K. Androsov^{a,28}, P. Azzurri^a, G. Bagliesi^a, J. Bernardini^a, T. Boccali^a, G. Broccolo^{a,c}, R. Castaldi^a, M. A. Ciocci^{a,28}, R. Dell'Orso^a, S. Donato^{a,c}, F. Fiori^{a,c}, L. Foà^{a,c}, A. Giassi^a, M. T. Grippo^{a,28}, A. Kraan^a, F. Ligabue^{a,c}, T. Lomtadze^a, L. Martina^{a,b}, A. Messineo^{a,b}, C. S. Moon^{a,29}, F. Palla^{a,2}, A. Rizzi^{a,b}, A. Savoy-Navarro^{a,30}, A. T. Serban^a, P. Spagnolo^a, P. Squillacioti^{a,28}, R. Tenchini^a, G. Tonelli^{a,b}, A. Venturi^a, P. G. Verdini^a, C. Vernieri^{a,c}

INFN Sezione di Roma^a, Università di Roma^b, Rome, Italy

L. Barone^{a,b}, F. Cavallari^a, D. Del Re^{a,b}, M. Diemoz^a, M. Grassi^{a,b}, C. Jorda^a, E. Longo^{a,b}, F. Margaroli^{a,b}, P. Meridiani^a, F. Micheli^{a,b}, S. Nourbakhsh^{a,b}, G. Organtini^{a,b}, R. Paramatti^a, S. Rahatlou^{a,b}, C. Rovelli^a, L. Soffi^{a,b}, P. Traczyk^{a,b}

INFN Sezione di Torino^a, Università di Torino^b, Università del Piemonte Orientale (Novara)^c, Turin, Italy

N. Amapane^{a,b}, R. Arcidiacono^{a,c}, S. Argiro^{a,b}, M. Arneodo^{a,c}, R. Bellan^{a,b}, C. Biino^a, N. Cartiglia^a, S. Casasso^{a,b}, M. Costa^{a,b}, A. Degano^{a,b}, N. Demaria^a, C. Mariotti^a, S. Maselli^a, E. Migliore^{a,b}, V. Monaco^{a,b}, M. Musich^a, M. M. Obertino^{a,c}, G. Ortona^{a,b}, L. Pacher^{a,b}, N. Pastrone^a, M. Pelliccioni^{a,2}, A. Potenza^{a,b}, A. Romero^{a,b}, M. Ruspa^{a,c}, R. Sacchi^{a,b}, A. Solano^{a,b}, A. Staiano^a, U. Tamponi^a

INFN Sezione di Trieste^a, Università di Trieste^b, Trieste, Italy

S. Belforte^a, V. Candelise^{a,b}, M. Casarsa^a, F. Cossutti^a, G. Della Ricca^{a,b}, B. Gobbo^a, C. La Licata^{a,b}, M. Marone^{a,b}, D. Montanino^{a,b}, A. Penzo^a, A. Schizzi^{a,b}, T. Umer^{a,b}, A. Zanetti^a

Kangwon National University, Chuncheon, Korea

S. Chang, T. Y. Kim, S. K. Nam

Kyungpook National University, Taegu, Korea

D. H. Kim, G. N. Kim, J. E. Kim, M. S. Kim, D. J. Kong, S. Lee, Y. D. Oh, H. Park, A. Sakharov, D. C. Son

Institute for Universe and Elementary Particles, Chonnam National University, Kwangju, Korea

J. Y. Kim, Zero J. Kim, S. Song

Korea University, Seoul, Korea

S. Choi, D. Gyun, B. Hong, M. Jo, H. Kim, Y. Kim, B. Lee, K. S. Lee, S. K. Park, Y. Roh

University of Seoul, Seoul, Korea

M. Choi, J. H. Kim, C. Park, I. C. Park, S. Park, G. Ryu

Sungkyunkwan University, Suwon, Korea

Y. Choi, Y. K. Choi, J. Goh, E. Kwon, J. Lee, H. Seo, I. Yu

Vilnius University, Vilnius, Lithuania

A. Juodagalvis

National Centre for Particle Physics, Universiti Malaya, Kuala Lumpur, Malaysia

J. R. Komaragiri

Centro de Investigacion y de Estudios Avanzados del IPN, Mexico City, Mexico

H. Castilla-Valdez, E. De La Cruz-Burelo, I. Heredia-de La Cruz³¹, R. Lopez-Fernandez, J. Martínez-Ortega, A. Sanchez-Hernandez, L. M. Villasenor-Cendejas

Universidad Iberoamericana, Mexico City, Mexico

S. Carrillo Moreno, F. Vazquez Valencia

Benemerita Universidad Autonoma de Puebla, Puebla, Mexico

H. A. Salazar Ibarquen

Universidad Autónoma de San Luis Potosí, San Luis Potosí, Mexico

E. Casimiro Linares, A. Morelos Pineda

University of Auckland, Auckland, New Zealand

D. Krofcheck

University of Canterbury, Christchurch, New Zealand

P. H. Butler, R. Doesburg, S. Reucroft

National Centre for Physics, Quaid-I-Azam University, Islamabad, Pakistan

A. Ahmad, M. Ahmad, M. I. Asghar, J. Butt, Q. Hassan, H. R. Hoorani, W. A. Khan, T. Khurshid, S. Qazi, M. A. Shah, M. Shoaib

National Centre for Nuclear Research, Swierk, Poland

H. Bialkowska, M. Bluj, B. Boimska, T. Frueboes, M. Górski, M. Kazana, K. Nawrocki, K. Romanowska-Rybinska, M. Szleper, G. Wrochna, P. Zalewski

Institute of Experimental Physics, Faculty of Physics, University of Warsaw, Warsaw, Poland

G. Brona, K. Bunkowski, M. Cwiok, W. Dominik, K. Doroba, A. Kalinowski, M. Konecki, J. Krolikowski, M. Misiura, W. Wolszczak

Laboratório de Instrumentação e Física Experimental de Partículas, Lisbon, Portugal

P. Bargassa, C. Beirão Da Cruz E Silva, P. Faccioli, P. G. Ferreira Parracho, M. Gallinaro, F. Nguyen, J. Rodrigues Antunes, J. Seixas, J. Varela, P. Vischia

Joint Institute for Nuclear Research, Dubna, Russia

I. Golutvin, V. Karjavin, V. Konoplyanikov, V. Korenkov, G. Kozlov, A. Lanev, A. Malakhov, V. Matveev³², V. V. Mitsyn, P. Moisenz, V. Palichik, V. Perelygin, S. Shmatov, S. Shulha, N. Skatchkov, V. Smirnov, E. Tikhonenko, A. Zarubin

Petersburg Nuclear Physics Institute, Gatchina (St. Petersburg), Russia

V. Golovtsov, Y. Ivanov, V. Kim³³, P. Levchenko, V. Murzin, V. Oreshkin, I. Smirnov, V. Sulimov, L. Uvarov, S. Vavilov, A. Vorobyev, An. Vorobyev

Institute for Nuclear Research, Moscow, Russia

Yu. Andreev, A. Dermenev, S. Gninenko, N. Golubev, M. Kirsanov, N. Krasnikov, A. Pashenkov, D. Tlisov, A. Toropin

Institute for Theoretical and Experimental Physics, Moscow, Russia

V. Epshteyn, V. Gavrilov, N. Lychkovskaya, V. Popov, G. Safronov, S. Semenov, A. Spiridonov, V. Stolin, E. Vlasov, A. Zhokin

P.N. Lebedev Physical Institute, Moscow, Russia

V. Andreev, M. Azarkin, I. Dremin, M. Kirakosyan, A. Leonidov, G. Mesyats, S. V. Rusakov, A. Vinogradov

Skobeltsyn Institute of Nuclear Physics, Lomonosov Moscow State University, Moscow, Russia

A. Belyaev, E. Boos, M. Dubinin⁷, L. Dudko, A. Ershov, A. Gribushin, V. Klyukhin, O. Kodolova, I. Lokhtin, S. Obraztsov, S. Petrushanko, V. Savrin, A. Snigirev

State Research Center of Russian Federation, Institute for High Energy Physics, Protvino, Russia

I. Azhgirey, I. Bayshev, S. Bitioukov, V. Kachanov, A. Kalinin, D. Konstantinov, V. Krychkin, V. Petrov, R. Ryutin, A. Sobol, L. Tourchanovitch, S. Troshin, N. Tyurin, A. Uzunian, A. Volkov

Faculty of Physics and Vinca Institute of Nuclear Sciences, University of Belgrade, Belgrade, Serbia

P. Adzic³⁴, M. Dordevic, M. Ekmedzic, J. Milosevic

Centro de Investigaciones Energéticas Medioambientales y Tecnológicas (CIEMAT), Madrid, Spain

M. Aguilar-Benitez, J. Alcaraz Maestre, C. Battilana, E. Calvo, M. Cerrada, M. Chamizo Llatas², N. Colino, B. De La Cruz, A. Delgado Peris, D. Domínguez Vázquez, C. Fernandez Bedoya, J. P. Fernández Ramos, A. Ferrando, J. Flix, M. C. Fouz, P. Garcia-Abia, O. Gonzalez Lopez, S. Goy Lopez, J. M. Hernandez, M. I. Josa, G. Merino, E. Navarro De Martino, A. Pérez-Calero Yzquierdo, J. Puerta Pelayo, A. Quintario Olmeda, I. Redondo, L. Romero, M. S. Soares, C. Willmott

Universidad Autónoma de Madrid, Madrid, Spain

C. Albajar, J. F. de Trocóniz, M. Missiroli

Universidad de Oviedo, Oviedo, Spain

H. Brun, J. Cuevas, J. Fernandez Menendez, S. Folgueras, I. Gonzalez Caballero, L. Lloret Iglesias

Instituto de Física de Cantabria (IFCA), CSIC-Universidad de Cantabria, Santander, Spain

J. A. Brochero Cifuentes, I. J. Cabrillo, A. Calderon, J. Duarte Campderros, M. Fernandez, G. Gomez, J. Gonzalez Sanchez, A. Graziano, A. Lopez Virto, J. Marco, R. Marco, C. Martinez Rivero, F. Matorras, F. J. Munoz Sanchez, J. Piedra Gomez, T. Rodrigo, A. Y. Rodríguez-Marrero, A. Ruiz-Jimeno, L. Scodellaro, I. Vila, R. Vilar Cortabitarte

CERN, European Organization for Nuclear Research, Geneva, Switzerland

D. Abbaneo, E. Auffray, G. Auzinger, M. Bachtis, P. Baillon, A. H. Ball, D. Barney, A. Benaglia, J. Bendavid, L. Benhabib, J. F. Benitez, C. Bernet⁸, G. Bianchi, P. Bloch, A. Bocci, A. Bonato, O. Bondu, C. Botta, H. Breuker, T. Camporesi, G. Cerminara, T. Christiansen, J. A. Coarasa Perez, S. Colafranceschi³⁵, M. D'Alfonso, D. d'Enterria, A. Dabrowski, A. David, F. De Guio, A. De Roeck, S. De Visscher, M. Dobson, N. Dupont-Sagorin, A. Elliott-Peisert, J. Eugster, G. Franzoni, W. Funk, M. Giffels, D. Gigi, K. Gill, D. Giordano, M. Girone, M. Giunta, F. Glege, R. Gomez-Reino Garrido, S. Gowdy, R. Guida, J. Hammer, M. Hansen, P. Harris, J. Hegeman, V. Innocente, P. Janot, E. Karavakis, K. Kousouris, K. Krajczar, P. Lecoq, C. Lourenço, N. Magini, L. Malgeri, M. Mannelli, L. Masetti, F. Meijers, S. Mersi, E. Meschi, F. Moortgat, M. Mulders, P. Musella, L. Orsini, E. Palencia Cortezon, L. Pape, E. Perez, L. Perrozzi, A. Petrilli, G. Petrucciani, A. Pfeiffer, M. Pierini, M. Pimiä, D. Piparo, M. Plagge, A. Racz, W. Reece, G. Rolandi³⁶, M. Rovere, H. Sakulin, F. Santanastasio, C. Schäfer, C. Schwick, S. Sekmen, A. Sharma, P. Siegrist, P. Silva, M. Simon, P. Sphicas³⁷, D. Spiga, J. Steggemann, B. Stieger, M. Stoye, D. Treille, A. Tsirou, G. I. Veres²⁰, J. R. Vlimant, H. K. Wöhri, W. D. Zeuner

Paul Scherrer Institut, Villigen, Switzerland

W. Bertl, K. Deiters, W. Erdmann, R. Horisberger, Q. Ingram, H. C. Kaestli, S. König, D. Kotlinski, U. Langenegger, D. Renker, T. Rohe

Institute for Particle Physics, ETH Zurich, Zurich, Switzerland

F. Bachmair, L. Bäni, L. Bianchini, P. Bortignon, M. A. Buchmann, B. Casal, N. Chanon, A. Deisher, G. Dissertori, M. Dittmar, M. Donegà, M. Dünser, P. Eller, C. Grab, D. Hits, W. Luster, B. Mangano, A. C. Marini, P. Martinez Ruiz del Arbol, D. Meister, N. Mohr, C. Nägeli³⁸, P. Nef, F. Nessi-Tedaldi, F. Pandolfi, F. Pauss, M. Peruzzi, M. Quittnat, L. Rebane, F. J. Ronga, M. Rossini, A. Starodumov³⁹, M. Takahashi, K. Theofilatos, R. Wallny, H. A. Weber

Universität Zürich, Zurich, Switzerland

C. AMSLER⁴⁰, M. F. Canelli, V. Chiochia, A. De Cosa, C. Favaro, A. Hinzmann, T. Hreus, M. Ivova Rikova, B. Kilminster, B. Millan Mejias, J. Ngadiuba, P. Robmann, H. Snoek, S. Taroni, M. Verzetti, Y. Yang

National Central University, Chung-Li, Taiwan

M. Cardaci, K. H. Chen, C. Ferro, C. M. Kuo, S. W. Li, W. Lin, Y. J. Lu, R. Volpe, S. S. Yu

National Taiwan University (NTU), Taipei, Taiwan

P. Bartalini, P. Chang, Y. H. Chang, Y. W. Chang, Y. Chao, K. F. Chen, P. H. Chen, C. Dietz, U. Grundler, W.-S. Hou, Y. Hsiung, K. Y. Kao, Y. J. Lei, Y. F. Liu, R.-S. Lu, D. Majumder, E. Petrakou, X. Shi, J. G. Shiu, Y. M. Tzeng, M. Wang, R. Wilken

Chulalongkorn University, Bangkok, Thailand

B. Asavapibhop, N. Suwonjandee

Cukurova University, Adana, Turkey

A. Adiguzel, M. N. Bakirci⁴¹, S. Cerci⁴², C. Dozen, I. Dumanoglu, E. Eskut, S. Girgis, G. Gokbulut, E. Gurpinar, I. Hos, E. Kangal, A. Kayis Topaksu, G. Onengut⁴³, K. Ozdemir, S. Ozturk⁴¹, A. Polatoz, K. Sogut⁴⁴, D. Sunar Cerci⁴², B. Tali⁴², H. Topakli⁴¹, M. Vergili

Physics Department, Middle East Technical University, Ankara, Turkey

I. V. Akin, T. Aliev, B. Bilin, S. Bilmis, M. Deniz, H. Gamsizkan, A. M. Guler, G. Karapinar⁴⁵, K. Ocalan, A. Ozpineci, M. Serin, R. Sever, U. E. Surat, M. Yalvac, M. Zeyrek

Bogazici University, Istanbul, Turkey

E. Gülmez, B. Isildak⁴⁶, M. Kaya⁴⁷, O. Kaya⁴⁷, S. Ozkorucuklu⁴⁸

Istanbul Technical University, Istanbul, Turkey

H. Bahtiyar⁴⁹, E. Barlas, K. Cankocak, Y. O. Günaydin⁵⁰, F. I. Vardarli, M. Yücel

National Scientific Center, Kharkov Institute of Physics and Technology, Kharkiv, Ukraine

L. Levchuk, P. Sorokin

University of Bristol, Bristol, UK

J. J. Brooke, E. Clement, D. Cussans, H. Flacher, R. Frazier, J. Goldstein, M. Grimes, G. P. Heath, H. F. Heath, J. Jacob, L. Kreczko, C. Lucas, Z. Meng, D. M. Newbold⁵¹, S. Paramesvaran, A. Poll, S. Senkin, V. J. Smith, T. Williams

Rutherford Appleton Laboratory, Didcot, UK

K. W. Bell, A. Belyaev⁵², C. Brew, R. M. Brown, D. J. A. Cockerill, J. A. Coughlan, K. Harder, S. Harper, J. Ilic, E. Olaiya, D. Petyt, C. H. Shepherd-Themistocleous, A. Thea, I. R. Tomalin, W. J. Womersley, S. D. Worm

Imperial College, London, UK

M. Baber, R. Bainbridge, O. Buchmuller, D. Burton, D. Colling, N. Cripps, M. Cutajar, P. Dauncey, G. Davies, M. Della Negra, W. Ferguson, J. Fulcher, D. Futyan, A. Gilbert, A. Guneratne Bryer, G. Hall, Z. Hatherell, J. Hays, G. Iles, M. Jarvis, G. Karapostoli, M. Kenzie, R. Lane, R. Lucas⁵¹, L. Lyons, A.-M. Magnan, J. Marrouche, B. Mathias, R. Nandi, J. Nash, A. Nikitenko³⁹, J. Pela, M. Pesaresi, K. Petridis, M. Pioppi⁵³, D. M. Raymond, S. Rogerson, A. Rose, C. Seez, P. Sharp[†], A. Sparrow, A. Tapper, M. Vazquez Acosta, T. Virdee, S. Wakefield, N. Wardle

Brunel University, Uxbridge, UK

J. E. Cole, P. R. Hobson, A. Khan, P. Kyberd, D. Leggat, D. Leslie, W. Martin, I. D. Reid, P. Symonds, L. Teodorescu, M. Turner

Baylor University, Waco, USA

J. Dittmann, K. Hatakeyama, A. Kasmi, H. Liu, T. Scarborough

The University of Alabama, Tuscaloosa, USA

O. Charaf, S. I. Cooper, C. Henderson, P. Rumerio

Boston University, Boston, USA

A. Avetisyan, T. Bose, C. Fantasia, A. Heister, P. Lawson, D. Lazic, C. Richardson, J. Rohlf, D. Sperka, J. St. John, L. Sulak

Brown University, Providence, USA

J. Alimena, S. Bhattacharya, G. Christopher, D. Cutts, Z. Demiragli, A. Ferapontov, A. Garabedian, U. Heintz, S. Jabeen, G. Kukartsev, E. Laird, G. Landsberg, M. Luk, M. Narain, M. Segala, T. Sinthuprasith, T. Speer, J. Swanson

University of California, Davis, Davis, USA

R. Breedon, G. Breto, M. Calderon De La Barca Sanchez, S. Chauhan, M. Chertok, J. Conway, R. Conway, P. T. Cox, R. Erbacher, M. Gardner, W. Ko, A. Kopecky, R. Lander, T. Miceli, M. Mulhearn, D. Pellett, J. Pilot, F. Ricci-Tam, B. Rutherford, M. Searle, S. Shalhout, J. Smith, M. Squires, M. Tripathi, S. Wilbur, R. Yohay

University of California, Los Angeles, USA

V. Andreev, D. Cline, R. Cousins, S. Erhan, P. Everaerts, C. Farrell, M. Felcini, J. Hauser, M. Ignatenko, C. Jarvis, G. Rakness, P. Schlein[†], E. Takasugi, V. Valuev, M. Weber

University of California, Riverside, Riverside, USA

J. Babb, R. Clare, J. Ellison, J. W. Gary, G. Hanson, J. Heilman, P. Jandir, F. Lacroix, H. Liu, O. R. Long, A. Luthra, M. Malberti, H. Nguyen, A. Shrinivas, J. Sturdy, S. Sumowidagdo, S. Wimpenny

University of California, San Diego, La Jolla, USA

W. Andrews, J. G. Branson, G. B. Cerati, S. Cittolin, R. T. D'Agnolo, D. Evans, A. Holzner, R. Kelley, D. Kovalskyi, M. Lebourgeois, J. Letts, I. Macneill, S. Padhi, C. Palmer, M. Pieri, M. Sani, V. Sharma, S. Simon, E. Sudano, M. Tadel, Y. Tu, A. Vartak, S. Wasserbaech⁵⁴, F. Würthwein, A. Yagil, J. Yoo

University of California, Santa Barbara, Santa Barbara, USA

D. Barge, J. Bradmiller-Feld, C. Campagnari, T. Danielson, A. Dishaw, K. Flowers, M. Franco Sevilla, P. Geffert, C. George, F. Golf, J. Incandela, C. Justus, R. Magaña Villalba, N. Mccoll, V. Pavlunin, J. Richman, R. Rossin, D. Stuart, W. To, C. West

California Institute of Technology, Pasadena, USA

A. Apresyan, A. Bornheim, J. Bunn, Y. Chen, E. Di Marco, J. Duarte, D. Kcira, A. Mott, H. B. Newman, C. Pena, C. Rogan, M. Spiropulu, V. Timciuc, R. Wilkinson, S. Xie, R. Y. Zhu

Carnegie Mellon University, Pittsburgh, USA

V. Azzolini, A. Calamba, R. Carroll, T. Ferguson, Y. Iiyama, D. W. Jang, M. Paulini, J. Russ, H. Vogel, I. Vorobiev

University of Colorado at Boulder, Boulder, USA

J. P. Cumalat, B. R. Drell, W. T. Ford, A. Gaz, E. Luiggi Lopez, U. Nauenberg, J. G. Smith, K. Stenson, K. A. Ulmer, S. R. Wagner

Cornell University, Ithaca, USA

J. Alexander, A. Chatterjee, J. Chu, N. Eggert, L. K. Gibbons, W. Hopkins, A. Khukhunaishvili, B. Kreis, N. Mirman, G. Nicolas Kaufman, J. R. Patterson, A. Ryd, E. Salvati, W. Sun, W. D. Teo, J. Thom, J. Thompson, J. Tucker, Y. Weng, L. Winstrom, P. Wittich

Fairfield University, Fairfield, USA

D. Winn

Fermi National Accelerator Laboratory, Batavia, USA

S. Abdullin, M. Albrow, J. Anderson, G. Apollinari, L. A. T. Bauerdick, A. Beretvas, J. Berryhill, P. C. Bhat, K. Burkett, J. N. Butler, V. Chetluru, H. W. K. Cheung, F. Chlebana, S. Cihangir, V. D. Elvira, I. Fisk, J. Freeman, Y. Gao, E. Gottschalk, L. Gray, D. Green, S. Grünendahl, O. Gutsche, D. Hare, R. M. Harris, J. Hirschauer, B. Hooberman, S. Jindariani, M. Johnson, U. Joshi, K. Kaadze, B. Klima, S. Kwan, J. Linacre, D. Lincoln, R. Lipton, J. Lykken, K. Maeshima, J. M. Marraffino, V. I. Martinez Outschoorn, S. Maruyama, D. Mason, P. McBride, K. Mishra, S. Mrenna, Y. Musienko³², S. Nahn, C. Newman-Holmes, V. O'Dell, O. Prokofyev, N. Ratnikova, E. Sexton-Kennedy, S. Sharma, W. J. Spalding, L. Spiegel, L. Taylor, S. Tkaczyk, N. V. Tran, L. Uplegger, E. W. Vaandering, R. Vidal, A. Whitbeck, J. Whitmore, W. Wu, F. Yang, J. C. Yun

University of Florida, Gainesville, USA

D. Acosta, P. Avery, D. Bourilkov, T. Cheng, S. Das, M. De Gruttola, G. P. Di Giovanni, D. Dobur, R. D. Field, M. Fisher, Y. Fu, I. K. Furic, J. Hugon, B. Kim, J. Konigsberg, A. Korytov, A. Kropivnitskaya, T. Kypreos, J. F. Low, K. Matchev, P. Milenovic⁵⁵, G. Mitselmakher, L. Muniz, A. Rinkevicius, L. Shchutska, N. Skhirtladze, M. Snowball, J. Yelton, M. Zakaria

Florida International University, Miami, USA

V. Gaultney, S. Hewamanage, S. Linn, P. Markowitz, G. Martinez, J. L. Rodriguez

Florida State University, Tallahassee, USA

T. Adams, A. Askew, J. Bochenek, J. Chen, B. Diamond, J. Haas, S. Hagopian, V. Hagopian, K. F. Johnson, H. Prosper, V. Veeraraghavan, M. Weinberg

Florida Institute of Technology, Melbourne, USA

M. M. Baarmand, B. Dorney, M. Hohlmann, H. Kalakhety, F. Yumiceva

University of Illinois at Chicago (UIC), Chicago, USA

M. R. Adams, L. Apanasevich, V. E. Bazterra, R. R. Betts, I. Bucinskaite, R. Cavanaugh, O. Evdokimov, L. Gauthier, C. E. Gerber, D. J. Hofman, S. Khalatyan, P. Kurt, D. H. Moon, C. O'Brien, C. Silkworth, P. Turner, N. Varelas

The University of Iowa, Iowa City, USA

U. Akgun, E. A. Albayrak⁴⁹, B. Bilki⁵⁶, W. Clarida, K. Dilsiz, F. Duru, M. Haytmyradov, J.-P. Merlo, H. Mermerkaya⁵⁷, A. Mestvirishvili, A. Moeller, J. Nachtman, H. Ogul, Y. Onel, F. Ozok⁴⁹, R. Rahmat, S. Sen, P. Tan, E. Tiras, J. Wetzel, T. Yetkin⁵⁸, K. Yi

Johns Hopkins University, Baltimore, USA

B. A. Barnett, B. Blumenfeld, S. Bolognesi, D. Fehling, A. V. Gritsan, P. Maksimovic, C. Martin, M. Swartz

The University of Kansas, Lawrence, USA

P. Baringer, A. Bean, G. Benelli, J. Gray, R. P. Kenny III, M. Murray, D. Noonan, S. Sanders, J. Sekaric, R. Stringer, Q. Wang, J. S. Wood

Kansas State University, Manhattan, USA

A. F. Barfuss, I. Chakaberia, A. Ivanov, S. Khalil, M. Makouski, Y. Maravin, L. K. Saini, S. Shrestha, I. Svintradze

Lawrence Livermore National Laboratory, Livermore, USA

J. Gronberg, D. Lange, F. Rebassoo, D. Wright

University of Maryland, College Park, USA

A. Baden, B. Calvert, S. C. Eno, J. A. Gomez, N. J. Hadley, R. G. Kellogg, T. Kolberg, Y. Lu, M. Marionneau, A. C. Mignerey, K. Pedro, A. Skuja, J. Temple, M. B. Tonjes, S. C. Tonwar

Massachusetts Institute of Technology, Cambridge, USA

A. Apyan, R. Barbieri, G. Bauer, W. Busza, I. A. Cali, M. Chan, L. Di Matteo, V. Dutta, G. Gomez Ceballos, M. Goncharov, D. Gulhan, M. Klute, Y. S. Lai, Y.-J. Lee, A. Levin, P. D. Luckey, T. Ma, C. Paus, D. Ralph, C. Roland, G. Roland, G. S. F. Stephens, F. Stöckli, K. Sumorok, D. Velicanu, J. Veverka, B. Wyslouch, M. Yang, A. S. Yoon, M. Zanetti, V. Zhukova

University of Minnesota, Minneapolis, USA

B. Dahmes, A. De Benedetti, A. Gude, S. C. Kao, K. Klapoetke, Y. Kubota, J. Mans, N. Pastika, R. Rusack, A. Singovsky, N. Tambe, J. Turkewitz

University of Mississippi, Oxford, USA

J. G. Acosta, L. M. Cremaldi, R. Kroeger, S. Oliveros, L. Perera, D. A. Sanders, D. Summers

University of Nebraska-Lincoln, Lincoln, USA

E. Avdeeva, K. Bloom, S. Bose, D. R. Claes, A. Dominguez, R. Gonzalez Suarez, J. Keller, D. Knowlton, I. Kravchenko, J. Lazo-Flores, S. Malik, F. Meier, G. R. Snow

State University of New York at Buffalo, Buffalo, USA

J. Dolen, A. Godshalk, I. Iashvili, S. Jain, A. Kharchilava, A. Kumar, S. Rappoccio

Northeastern University, Boston, USA

G. Alverson, E. Barberis, D. Baumgartel, M. Chasco, J. Haley, A. Massironi, D. Nash, T. Orimoto, D. Trocino, D. Wood, J. Zhang

Northwestern University, Evanston, USA

A. Anastassov, K. A. Hahn, A. Kubik, L. Lusito, N. Mucia, N. Odell, B. Pollack, A. Pozdnyakov, M. Schmitt, S. Stoynev, K. Sung, M. Velasco, S. Won

University of Notre Dame, Notre Dame, USA

D. Berry, A. Brinkerhoff, K. M. Chan, A. Drozdetskiy, M. Hildreth, C. Jessop, D. J. Karmgard, N. Kellams, J. Kolb, K. Lannon, W. Luo, S. Lynch, N. Marinelli, D. M. Morse, T. Pearson, M. Planer, R. Ruchti, J. Slaunwhite, N. Valls, M. Wayne, M. Wolf, A. Woodard

The Ohio State University, Columbus, USA

L. Antonelli, B. Bylsma, L. S. Durkin, S. Flowers, C. Hill, R. Hughes, K. Kotov, T. Y. Ling, D. Puigh, M. Rodenburg, G. Smith, C. Vuosalu, B. L. Winer, H. Wolfe, H. W. Wulsin

Princeton University, Princeton, USA

E. Berry, P. Elmer, V. Halyo, P. Hebda, A. Hunt, P. Jindal, S. A. Koay, P. Lujan, D. Marlow, T. Medvedeva, M. Mooney, J. Olsen, P. Piroué, X. Quan, A. Raval, H. Saka, D. Stickland, C. Tully, J. S. Werner, S. C. Zenz, A. Zuranski

University of Puerto Rico, Mayagüez, USA

E. Brownson, A. Lopez, H. Mendez, J. E. Ramirez Vargas

Purdue University, West Lafayette, USA

E. Alagoz, D. Benedetti, G. Bolla, D. Bortoletto, M. De Mattia, A. Everett, Z. Hu, M. K. Jha, M. Jones, K. Jung, M. Kress, N. Leonardo, D. Lopes Pegna, V. Maroussov, P. Merkel, D. H. Miller, N. Neumeister, B. C. Radburn-Smith, I. Shipsey, D. Silvers, A. Svyatkovskiy, F. Wang, W. Xie, L. Xu, H. D. Yoo, J. Zablocki, Y. Zheng

Purdue University Calumet, Hammond, USA

N. Parashar

Rice University, Houston, USA

A. Adair, B. Akgun, K. M. Ecklund, F. J. M. Geurts, W. Li, B. Michlin, B. P. Padley, R. Redjimi, J. Roberts, J. Zabel

University of Rochester, Rochester, USA

B. Betchart, A. Bodek, R. Covarelli, P. de Barbaro, R. Demina, Y. Eshaq, T. Ferbel, A. Garcia-Bellido, P. Goldenzweig, J. Han, A. Harel, D. C. Miner, G. Petrillo, D. Vishnevskiy, M. Zielinski

The Rockefeller University, New York, USA

A. Bhatti, R. Ciesielski, L. Demortier, K. Goulios, G. Lungu, S. Malik, C. Mesropian

Rutgers, The State University of New Jersey, Piscataway, USA

S. Arora, A. Barker, J. P. Chou, C. Contreras-Campana, E. Contreras-Campana, D. Duggan, D. Ferencek, Y. Gershtein, R. Gray, E. Halkiadakis, D. Hidas, A. Lath, S. Panwalkar, M. Park, R. Patel, V. Rekovic, J. Robles, S. Salur, S. Schnetzer, C. Seitz, S. Somalwar, R. Stone, S. Thomas, P. Thomassen, M. Walker

University of Tennessee, Knoxville, USA

K. Rose, S. Spanier, Z. C. Yang, A. York

Texas A&M University, College Station, USA

O. Bouhali⁵⁹, R. Eusebi, W. Flanagan, J. Gilmore, T. Kamon⁶⁰, V. Khotilovich, V. Krutelyov, R. Montalvo, I. Osipenkov, Y. Pakhotin, A. Perloff, J. Roe, A. Safonov, T. Sakuma, I. Suarez, A. Tatarinov, D. Toback

Texas Tech University, Lubbock, USA

N. Akchurin, C. Cowden, J. Damgov, C. Dragoiu, P. R. Duderod, J. Faulkner, K. Kovitanggoon, S. Kunori, S. W. Lee, T. Libeiro, I. Volobouev

Vanderbilt University, Nashville, USA

E. Appelt, A. G. Delannoy, S. Greene, A. Gurrola, W. Johns, C. Maguire, Y. Mao, A. Melo, M. Sharma, P. Sheldon, B. Snook, S. Tuo, J. Velkovska

University of Virginia, Charlottesville, USA

M. W. Arenton, S. Boutle, B. Cox, B. Francis, J. Goodell, R. Hirosky, A. Ledovskoy, H. Li, C. Lin, C. Neu, J. Wood

Wayne State University, Detroit, USA

S. Gollapinni, R. Harr, P. E. Karchin, C. Kottachchi Kankanamge Don, P. Lamichhane

University of Wisconsin, Madison, USA

D. A. Belknap, L. Borrello, D. Carlsmith, M. Cepeda, S. Dasu, S. Duric, E. Friis, M. Grothe, R. Hall-Wilton, M. Herndon, A. Hervé, P. Klabbers, J. Klukas, A. Lanaro, C. Lazaridis, A. Levine, R. Loveless, A. Mohapatra, I. Ojalvo, T. Perry, G. A. Pierro, G. Polese, I. Ross, T. Sarangi, A. Savin, W. H. Smith, N. Woods

† Deceased

- 1: Also at Vienna University of Technology, Vienna, Austria
- 2: Also at CERN, European Organization for Nuclear Research, Geneva, Switzerland
- 3: Also at Institut Pluridisciplinaire Hubert Curien, Université de Strasbourg, Université de Haute Alsace Mulhouse, CNRS/IN2P3, Strasbourg, France
- 4: Also at National Institute of Chemical Physics and Biophysics, Tallinn, Estonia
- 5: Also at Skobeltsyn Institute of Nuclear Physics, Lomonosov Moscow State University, Moscow, Russia
- 6: Also at Universidade Estadual de Campinas, Campinas, Brazil
- 7: Also at California Institute of Technology, Pasadena, USA
- 8: Also at Laboratoire Leprince-Ringuet, Ecole Polytechnique, IN2P3-CNRS, Palaiseau, France
- 9: Also at Suez University, Suez, Egypt
- 10: Also at British University in Egypt, Cairo, Egypt
- 11: Also at Cairo University, Cairo, Egypt
- 12: Also at Fayoum University, El-Fayoum, Egypt
- 13: Also at Helwan University University, Cairo, Egypt
- 14: Now at Ain Shams University, Cairo, Egypt
- 15: Also at Université de Haute Alsace, Mulhouse, France
- 16: Also at Joint Institute for Nuclear Research, Dubna, Russia
- 17: Also at Brandenburg University of Technology, Cottbus, Germany
- 18: Also at The University of Kansas, Lawrence, USA
- 19: Also at Institute of Nuclear Research ATOMKI, Debrecen, Hungary
- 20: Also at Eötvös Loránd University, Budapest, Hungary
- 21: Now at King Abdulaziz University, Jeddah, Saudi Arabia
- 22: Also at University of Visva-Bharati, Santiniketan, India
- 23: Also at University of Ruhuna, Matara, Sri Lanka

- 24: Also at Isfahan University of Technology, Isfahan, Iran
- 25: Also at Sharif University of Technology, Tehran, Iran
- 26: Also at Plasma Physics Research Center, Science and Research Branch, Islamic Azad University, Tehran, Iran
- 27: Also at Laboratori Nazionali di Legnaro dell'INFN, Legnaro, Italy
- 28: Also at Università degli Studi di Siena, Siena, Italy
- 29: Also at Centre National de la Recherche Scientifique (CNRS)-IN2P3, Paris, France
- 30: Also at Purdue University, West Lafayette, USA
- 31: Also at Universidad Michoacana de San Nicolas de Hidalgo, Morelia, Mexico
- 32: Also at Institute for Nuclear Research, Moscow, Russia
- 33: Also at St. Petersburg State Polytechnical University, St. Petersburg, Russia
- 34: Also at Faculty of Physics, University of Belgrade, Belgrade, Serbia
- 35: Also at Facoltà Ingegneria, Università di Roma, Rome, Italy
- 36: Also at Scuola Normale e Sezione dell'INFN, Pisa, Italy
- 37: Also at University of Athens, Athens, Greece
- 38: Also at Paul Scherrer Institut, Villigen, Switzerland
- 39: Also at Institute for Theoretical and Experimental Physics, Moscow, Russia
- 40: Also at Albert Einstein Center for Fundamental Physics, Bern, Switzerland
- 41: Also at Gaziosmanpasa University, Tokat, Turkey
- 42: Also at Adiyaman University, Adiyaman, Turkey
- 43: Also at Cag University, Mersin, Turkey
- 44: Also at Mersin University, Mersin, Turkey
- 45: Also at Izmir Institute of Technology, Izmir, Turkey
- 46: Also at Ozyegin University, Istanbul, Turkey
- 47: Also at Kafkas University, Kars, Turkey
- 48: Also at Istanbul University, Faculty of Science, Istanbul, Turkey
- 49: Also at Mimar Sinan University, Istanbul, Istanbul, Turkey
- 50: Also at Kahramanmaras Sütcü Imam University, Kahramanmaras, Turkey
- 51: Also at Rutherford Appleton Laboratory, Didcot, UK
- 52: Also at School of Physics and Astronomy, University of Southampton, Southampton, UK
- 53: Also at INFN Sezione di Perugia; Università di Perugia, Perugia, Italy
- 54: Also at Utah Valley University, Orem, USA
- 55: Also at University of Belgrade, Faculty of Physics and Vinca Institute of Nuclear Sciences, Belgrade, Serbia
- 56: Also at Argonne National Laboratory, Argonne, USA
- 57: Also at Erzincan University, Erzincan, Turkey
- 58: Also at Yildiz Technical University, Istanbul, Turkey
- 59: Also at Texas A&M University at Qatar, Doha, Qatar
- 60: Also at Kyungpook National University, Taegu, Korea